Positron Spectrum from the Decay of the μ Meson*

WALTER F. DUDZIAK,† RYOKICHI SAGANE,‡ AND JAMES VEDDER§
Radiation Laboratory, University of California, Berkeley, California
(Received October 20, 1958)

A magnetic spiral-orbit spectrometer was used to study the positron spectrum from an isotropic μ^+ decay. The detected positrons were identified by an electronic technique designed to measure the lifetime of the muon. Our measured weighted mean value of the μ^+ mean life is $\tau_\mu = 2.21 \pm 0.02$ μsec.

The data have been analyzed according to the simplified one-parameter theory of Michel, as modified by Behrends, Finkelstein, and Sirlin and corrected by Berman to include radiative corrections to the muon decay theory. We obtained $\rho_M = 0.741 \pm 0.027$ for the Michel parameter as the weighted mean value from four experiments. In these experiments the measurements in the low-energy positron region were not of sufficient accuracy to yield an estimate of the second Michel parameter.

Included is a measurement of the maximum positron energy. The weighted mean value of this measurement is $W = 52.87 \pm 0.07$ Mev. From this value and its simple algebraic relation to the masses of the decay particles one obtains a value of the μ^+ mass $\mu = 206.94 \pm 0.27$.

Tables of the radiative correction to muon decay are given as well as the total corrections that must be added to the Michel parameter that is derived from experimental data by using the simple Michel theory without radiative corrections. For the energy region of the majority of experiments from which the ρ_M value is determined, this total correction in $\Delta\rho$ is approximately 0.040.

From our measured value of the maximum positron energy, an estimate is made of the possible upper limit on the mass of the neutral particle in muon decay. This upper limit is reported as 8 electron-mass units.

INTRODUCTION

EARLY observations of the energy of electrons from the decay of the muon have guided theoretical calculations through the many proposed assumptions for the possible mode of decay of the muon. From the experimental point of view, the most successful theoretical calculations were based on the assumption of a direct interaction between four fermions, i.e., on

$$\mu^\pm \rightarrow e^\pm + \nu_1 + \nu_2.$$

Using this assumption for the decay scheme of the muon and the mechanics first proposed by Fermi for describing β decay, Tiomno and Wheeler[1] and Michel[2] have predicted the probable energy dependence of the $e^\pm$ in muon decay for this process. Michel, in particular, calculated the energy distribution of the positrons from the isotropic μ-meson decay, using a linear combination of all five interactions (i.e., scalar, vector, tensor, axial vector, and pseudoscalar) for both distinguishable and indistinguishable neutrinos. These calculations led Michel to the following general expression for the energy-dependent probability of $e^\pm$ emission in isotropic μ-meson decay:

$$P(E)dE = \frac{(E^2-\epsilon^2)^{\frac{1}{2}}}{3\hbar(2\pi\hbar^2c^2)^3}\mu[3E(W-E)K_1 + 2(E^2-\epsilon^2)K_2 + 3\epsilon(W-E)K_3]dE, \quad (1)$$

where K_1, K_2, and K_3 are functions of the five Fermi coupling constants, i.e.,

$$\begin{aligned} K_1 &= g_S^2 + 2(g_V^2 + g_T^2 + g_A^2) + g_P^2, \\ K_2 &= g_V^2 + 2g_T^2 + g_A^2, \\ K_3 &= g_S^2 - 2g_V^2 + 2g_A^2 - g_P^2. \end{aligned} \quad (2)$$

E and W are the total energy and maximum energy of the positron, and ϵ and μ are, respectively, the electron and muon rest mass. This transition probability can easily be rewritten in terms of two parameters that are bilinear functions of the five coupling constants:

$$P(E)dE = \frac{1}{\tau_\mu}\frac{(E^2-\epsilon^2)^{\frac{1}{2}}}{A+\psi B}[3E(W-E) + \tfrac{2}{3}\rho_M(4E^2-3EW-\epsilon^2) + 3\psi\epsilon(W-E)]dE, \quad (3)$$

where $\rho_M = 3K_2/(K_1+2K_2)$ and is limited to the range of values $0 \leqslant \rho_M \leqslant 1$, and $\psi = K_3/(K_1+2K_2)$ and is limited to the range of values $-1 \leqslant \psi \leqslant 1$. The terms A and B are constants that depend on the value of W. (Note: ψ = Michel's η. We reserve η so as to conform with the notation in Behrends *et al.*[3] and Berman[4].) Thus the Michel theory predicts a family of possible energy spectra for the positrons from an isotropic positive muon decay, each of which has two free parameters that may in principle be determined experimentally. In addition to these two parameters, two other measurements can be made. These are (a) the maximum energy W and (b) the mean lifetime of the muon, τ_μ. A meas-

* Work done under the auspices of the U. S. Atomic Energy Commission.
† Present address: TEMPO, Santa Barbara, California.
‡ Present address: Japanese Atomic Energy Commission, Research Institute, Shimbashi, Tokyo, Japan.
§ Present address: Lockheed Missiles Systems Division, Palo Alto, California.
[1] J. Tiomno and J. A. Wheeler, Revs. Modern Phys. **21**, 144 (1949).
[2] L. Michel, Proc. Phys. Soc. (London) **A53**, 514 (1950); thesis, University of Paris, 1953 (unpublished).
[3] Behrends, Finkelstein, and Sirlin, Phys. Rev. **101**, 866 (1956).
[4] S. M. Berman, "Radiative Corrections to Muon Decay," memorandium, California Institute of Technology (unpublished); (also private communication). The correction used here omits the last term presented in this reference. The author likewise omitted this term in his published paper [Phys. Rev. **112**, 267 (1958)].

urement of W becomes a measurement of the muon rest mass μ because W is related to the rest masses of the interacting fermions by the expression $W=(\mu^2+\epsilon^2)/2\mu$ when the assumption is made that the neutrino rest mass, ν, is 0. The purpose of this experiment was to measure these four quantities.

We succeeded in determining three of these parameters—that is, in measuring τ_μ, ρ_M, and W. In what follows we deal with details of these measurements. However, a few remarks should be made about our efforts to measure the ψ parameter.

Consider the effect of ψ on the shape of the positron decay spectrum as shown by Eq. (3) [even though ψ, like ρ_M, no longer has this simple meaning when radiative corrections are considered in deriving the transition probability, Eq. (1); these corrections were ignored in the derivation of Eq. (1)]. The effect of ψ on the shape of the spectrum increases as the positron energy decreases. Calculations summarized in Table I show that the difference in the ratios of the positron intensities $[P(E=10)/P(E=5)]_\psi=Q_\psi$, when evaluated at 5 Mev and 10 Mev for two ψ values at the same ρ_M value, can be as large as 10%. This is a measurable difference.

In our experiment we obtained the ratios from the intensity measurements at three positron energies in this low-energy region. The lowest positron energy at which measurements were made was 5 Mev. In the reduction of these data we found that the background contribution to the measured intensity was comparable to the contribution arising from positrons leaving the target. Because there is some ambiguity in determining the magnitude of this background in the very-low-energy region (Appendix D), we feel that these intensity measurements are not reliable. Therefore they are omitted in the presentation of our data and no estimate is made of the value of the ψ parameter.

EXPERIMENTAL PROCEDURE

The measurements of τ_M, ρ_M, and W arise from experiments[5] summarized in Table II and are related to the same general experimental procedure. Except for target modifications and other parameters that affect the resolution of the spectrometer, the procedure was the same. We discuss it here in a general way and present the details in the Appendixes and in a Laboratory report.[6]

TABLE I. Ratios of $Q=P(E=10)/P(E=5)$ for different ψ values.

ρ_M	Calculated ratio for value of Q at $\psi=-1$ to value at $\psi=0$	Calculated ratio for value of Q at $\psi=0$ to value at $\psi=+1$
0.50	1.088	1.070
0.70	1.115	1.086
0.75	1.146	1.092

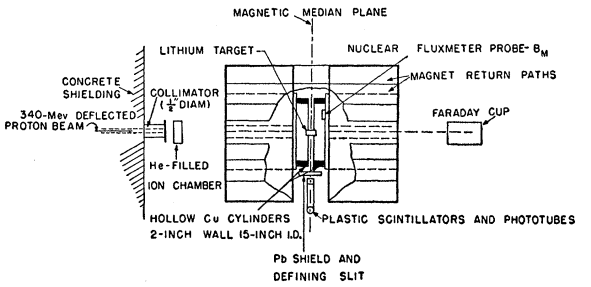

FIG. 1. Schematic diagram of the experimental arrangement.

Each measurement was made by using a spiral-orbit spectrometer[7–12] for determining the momentum distribution, and a quadruple-coincidence electronic technique for identification of positrons from a muon decay.

Figures 1, 2, and 3 represent schematically the general features of our procedure. As shown in Fig. 1, a pulsed proton beam was introduced along the magnetic axis of a spiral-orbit spectrometer. It was used to create pions in a lithium target that was mounted coaxially with the magnetic axis. Those pions that were created with insufficient energy to emerge from the target decayed inside the target into muons that in turn disintegrated, giving birth to positrons. The energy spectrum from this positron source was magnetically analyzed by means of the spiral-orbit principle, as shown in Fig. 2.

Positrons were detected as quadruple coincidences of signals from four plastic scintillators (three were 3 by 3 by $\frac{1}{4}$ in., and the fourth one 4 by 4 by $\frac{1}{2}$ in.). As illustrated in Fig. 3, counts were taken between proton pulses during four consecutive gates each having a 2-microsecond width. The start of the first gate was delayed by 3 μsec relative to a proton pulse. The full width of each

[5] These experiments were conducted during August and September, 1955. The analysis of the data is primarily the effort of one of us (W.F.D.). It does not utilize data obtained prior to this time. The analysis was delayed by (a) the departure from the Laboratory of one of us (R.S.) following the completion of the experiment, (b) the involvement of the other two authors in other experiments, and (c) the time required to develop and numerically check the correctness of the computer programs that are used in the analysis of the data. The results of Experiment A were presented at the 1956 Physical Society meeting in Washington (see reference 16). The analyzed results of Experiments B(a) and B(b) were presented by W. H. Barkas at the *Seventh Annual Rochester Conference on High-Energy Physics, April 15–19, 1957* (Interscience Publishers, New York, 1957).

[6] Dudziak, Sagane, and Vedder, University of California Radiation Laboratory Report UCRL-8202 and supplement March and June, 1958 (unpublished).

[7] G. Miyamoto, Proc. Phys.-Math. Soc. Japan (in Japanese) **17**, 557 (1943).

[8] Iwata, Miyamoto, and Kotani, J. Phys. Soc. Japan **2**, 1 (1947) [in Japanese; English translation by Ryokichi Sagane, University of California Radiation Laboratory Report UCRL-111 (unpublished)].

[9] Sagane, Miyamoto, Nakamura, and Takechi, Proc. Phys.-Math. Soc. Japan **25**, 274 (1943).

[10] M. Sakai, J. Phys. Soc. Japan **5**, 178 (1950); J. phys. radium **14**, 570 (1953).

[11] Walter Dudziak, (thesis, University of California Radiation Laboratory Report UCRL-3564) April, 1954 (unpublished).

[12] V. S. Shpinel and O. Sh. Grois, Zhur. Tekh. Fiz. **26**, No. 10, 2259 (1956). (In Russian.)

TABLE II. Summary of experiments conducted and experimental conditions.

	Type of experiment		Experimental geometry: Cylindrical target Type	Cylindrical target Diameter (in.)	Spectrometer slit, Θ' (deg)	Proton beam diameter (in.)
A	Measurement of the Michel parameter, ρ_M	By ratios from intensities at three energies $E'=39.84$, 46.96, and 48.72 Mev (minimum of 25 repeated measurements at each energy)	Li	(a) $2\frac{3}{8}$ (b) 1	25 25	$\frac{3}{4}$ $\frac{1}{2}$
B	Measurement of the Michel parameter, ρ_M	By measuring the spectrum (minimum of 10 repeated measurements at each energy)	Li	(a) $2\frac{3}{8}$ (b) $2\frac{3}{8}$ (c) $2\frac{3}{8}$ (d) 1 (e) 1	25 25 35 25 35	$\frac{3}{4}$ $\frac{1}{2}$ $\frac{1}{2}$ $\frac{1}{2}$ $\frac{1}{2}$
C	Measurement of the maximum positron energy, W	By spectrum measurements near the end point (minimum of 10 repeated measurements at each energy)	Be Be Li	(a) $\frac{1}{2}$ (b) $1\frac{1}{2}$ (c) $\frac{5}{8}-\frac{1}{4}$	35 35 35	1 $1\frac{1}{2}$ 1

proton pulse was <0.5 μsec. This counting procedure enabled us to use the same counts that determined the shape of the electron spectrum from the muon decay for a measure of τ_μ. The 3-μsec delay after a proton pulse was sufficient to decrease to $<2\%$ the accidental background at our highest counting rate and largest possible proton pulse. This background is defined as the count measured by introducing a 1-inch lead positron stopper between scintillators 2 and 3. During the course of the experiment the magnitude of an average proton pulse was $\leqslant\frac{1}{2}$ the pulse responsible for this background.

To eliminate errors in counting rate during the first gate that would be caused by insufficient recovery time from voltage overload brought about by secondaries

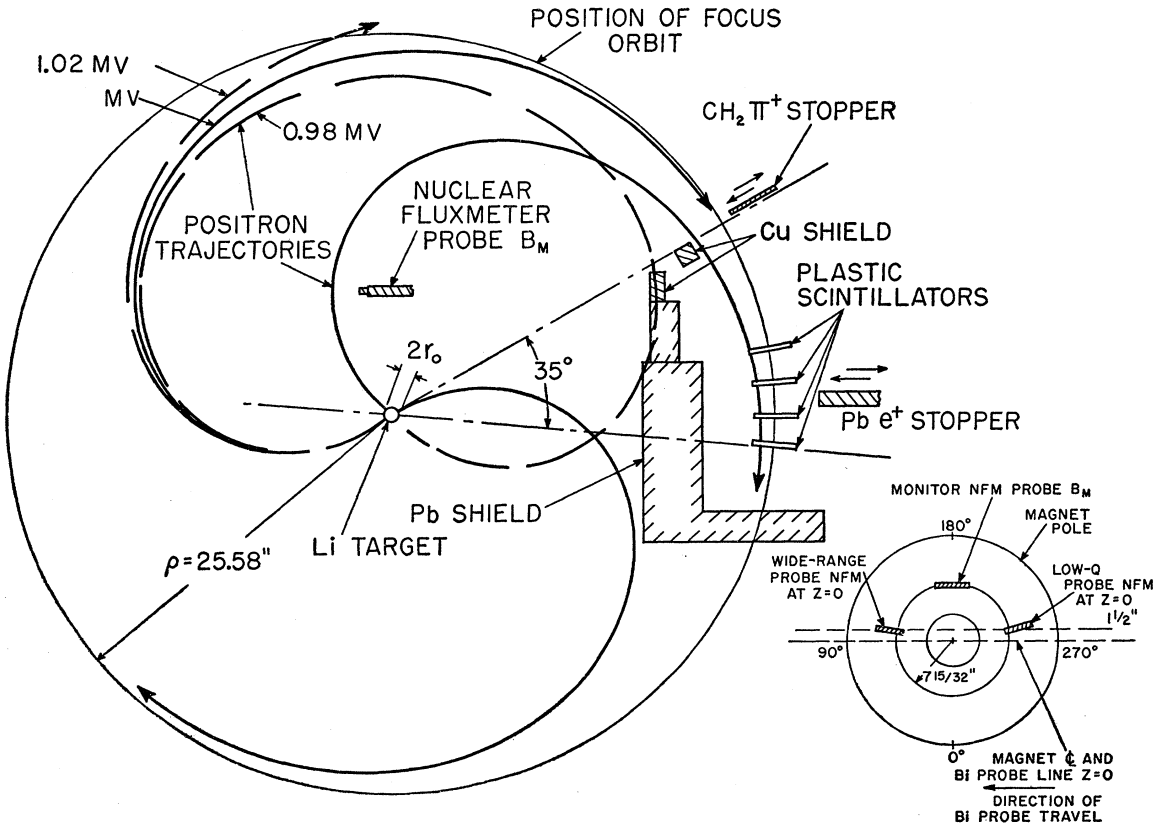

FIG. 2. Left: section at the median plane of the spectrometer for the muon experimental geometry. Right, below: schematic diagram of experimental arrangement used to measure the radial magnetic-field distribution.

produced during the proton pulse, we used (a) a negative voltage pulse applied to the second dynode of each photomultiplier during the time of the proton pulse (illustrated in Fig. 3), (b) a series of pulse-height limiters, and (c) a modified slow amplifier giving a moderately fast recovery—that is, from 2 to 2.5 μsec after a maximum proton pulse overload that occurred in the absence of (a) and (b). Normally this would have been about 15 μsec.

Effects of temperature variations on all electronic components were studied. Components that could not withstand the day-to-day temperature variations without drifting were enclosed in a temperature-controlled atmosphere held constant to within 1°C. These precautions eliminated drifts and permitted even day-to-day reproducibility of the adopted standard check points. In addition, a continuous check on the reliability of the tandem gate circuit was obtained by splitting the

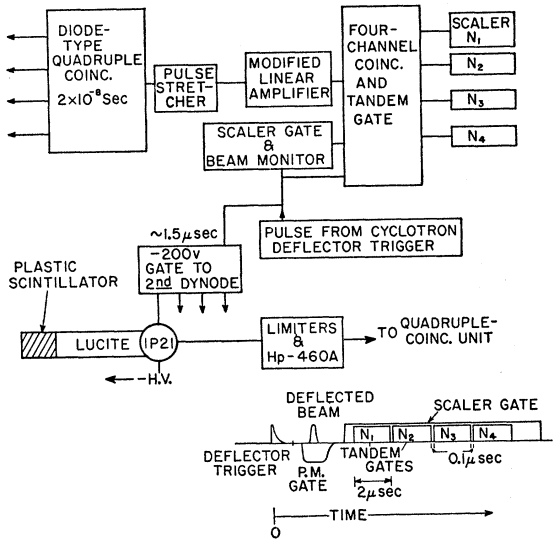

FIG. 3. Block diagram of the electronic gates and timing system.

pulse from the modified linear amplifier, and passing one part of it through a variable gate and then through a second tandem gate unit. (This is not shown in Fig. 3.) A variable gate has the property of converting any pulse above a present pulse height into a constant-output voltage pulse that has a fixed shape. Other standard electronic tests were made on variations that could introduce systematic errors into our results. These included measurements of (a) counting-rate uniformity across the surface of each scintillator, (b) high-voltage plateaus on each photomultiplier, (c) effect of magnetic-field variation on photomultipliers in magnetic shields (this test covered twice the magnetic-field variations that occurred during the experiment), (d) cable-length plateaus of the fast-electronics system, and (e) proton-monitor plateaus. We found that under certain proton beam conditions argon-filled ion chambers[11] gave false indications of the true number of protons. We attribute this to recombination in the highly ionized regions of the gas resulting from the passage of an intense proton pulse. For this reason we used a modified helium-ion chamber in tandem with a Faraday cup. This permitted a continuous check of our proton monitor, which was found accurate for variations of a factor of nine in the proton-beam intensity. No such variations of the proton beam intensity were allowed to occur during the course of our experiment.

MEASUREMENT OF THE MUON MEAN LIFE

The data presented in this paper (experiments *A* and *B*, Table II) as a measure of the Michel parameter were obtained during twelve different days. For each day the counts obtained during each gate were also added together. From this sum the accidental background for that gate was subtracted and then divided by the proper time width of the gate. By means of the method of least squares[13] we fitted a straight line to the semilog plot of the results from the four gates, and obtained the most probable value for the slope of the linear equation that determines the mean life of the muon, τ_μ. We also calculated the standard deviations of the constants defining the linear form of the equation. The mean life obtained from these calculations is displayed in Column 2 of Table III as the mean life measured by the counts for that particular day. Column 3 of Table III represents the corresponding standard deviation obtained from a statistical treatment of the data for that day. Basing the weights on the statistical errors as given in Column 3, one obtains $\tau_\mu=2.210\pm0.015$ μsec for the weighted mean value of the positive muon mean life. (For calibration of time scale see Appendix E.) We round off this value to $\tau_\mu=2.21\pm0.02$ in order to account partially for possible unknown systematic errors.

MEASUREMENT OF THE MICHEL PARAMETER ρ_M

A value of the Michel ρ_M parameter can be determined (a) from a measure of a ratio of the counting

TABLE III. Measurement of the mean life of the μ meson.

Trial	τ_μ (μsec)	$\sigma(\tau_\mu)$ (μsec)
1	2.208	0.022
2	2.277	0.045
3	2.220	0.086
4	2.224	0.075
5	2.224	0.041
6	2.216	0.047
7	2.168	0.108
8	2.184	0.072
9	2.168	0.080
10	2.175	0.065
11	2.146	0.081
12	2.159	0.070

Weighted statistical mean value $=\bar{\tau}_\mu=2.210\pm0.015$ μsec

[13] Raymond T. Birge, Phys. Rev. **40**, 207 (1932); Am. J. Phys. **7**, 351 (1939).

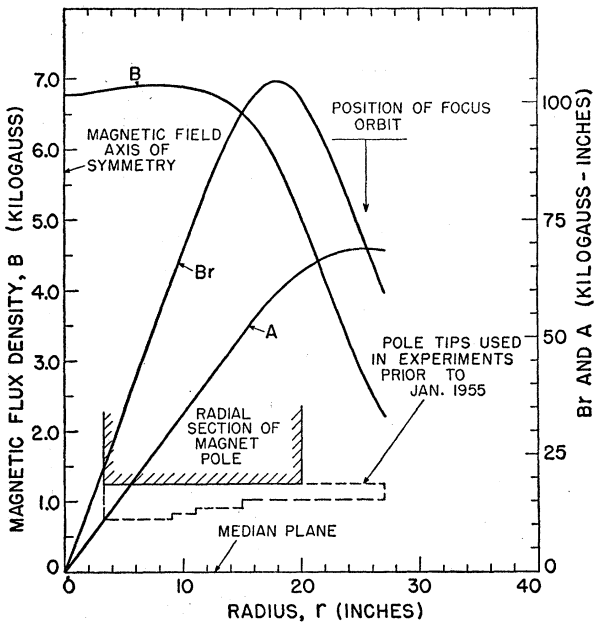

FIG. 4. Radial plot at one energy setting of the measured magnetic-field density and calculated vector potential in the median plane of the spectrometer.

rates at two positron energies near the high-energy end of the spectrum[14] or (b) from the measured shape of the positron decay spectrum. As shown in Table II, both these methods were used. The first of these methods is inferior to the second because of the greater influence of possible unknown systematic errors on the measurement of this Michel parameter (see reference 6). For this reason the data obtained in the Type A experiment listed in Table II were combined as part of the data of the Type B experiment and treated together. For each of these methods a momentum-analyzed positron beam arising from the decay of the muon is necessary. The momentum analysis was obtained by a new type of magnetic spectrometer that permits large-solid-angle focussing with good resolution (Appendix A). This spectrometer property arises from a nonuniform radial magnetic field (as shown in Fig. 4) that is symmetric about the magnetic axis (and therefore also about the axis of a cylindrical source that is placed coincident with it). The position of the focus orbit is determined by the shape of the magnetic-field distribution. This shape must remain unchanged if the focus-orbit position is to remain unchanged when the magnitude of the magnetic field is varied. In this spectrometer the resolution is very sensitive to very small changes in the shape of the magnetic field near the focus orbit. With the aid of improved magnetic measuring techniques (see Fig. 2), permitting a continuous display of radial position and the corresponding magnetic field at that radial position, we have found that there were small variations in field shape during our earlier measurements of the high-energy region of the μ-meson decay spectrum (Appendix B). Hence a large systematic error was introduced by these variations into the preliminary report of our early measurements.[15] From extensive experimental tests, which included a study of the corrections necessary for the previously reported measurements, we conclude that these difficulties were corrected by our reshaping of the magnetic field (Appendix B) and therefore did not affect the subsequent measurements that are summarized in Table II.

As shown in Fig. 2, the magnitude of the magnetic field was established by the frequency setting of a nuclear fluxmeter that was located in the flat region of the magnetic-field distribution. By calibration, each frequency setting was related to the vector potential at the focus orbit. We define E_0' as the total positron energy that is obtained from this vector potential at the focus orbit. During each intensity measurement the magnetic field at the position of the nuclear fluxmeter was continuously monitored. Our magnet-current regulation was such that a drift of only ± 1 gauss in 7000 gauss was observed during this measurement. From this and the calibration methods that were used (Fig. 2) we estimate that the accuracy of the absolute value of each E_0' setting is better than 0.2%.

Figures 5 and 6 summarize the raw experimental data obtained in our measurements of the Michel ρ_M parameter by the two different methods. These were the data used in Table III to yield a measure of the mean life of the muon. (By "raw data" at an E_0' energy we mean actual counts minus accidental background—previously defined and very small—per unit proton monitor, divided by the vector potential that corresponds to the frequency setting of E_0' by a nuclear fluxmeter.) The plotted errors are standard deviations as obtained by the rule of propagation of errors.

As shown by Table II and these figures, our data for measuring ρ_M from the shape of the spectrum were

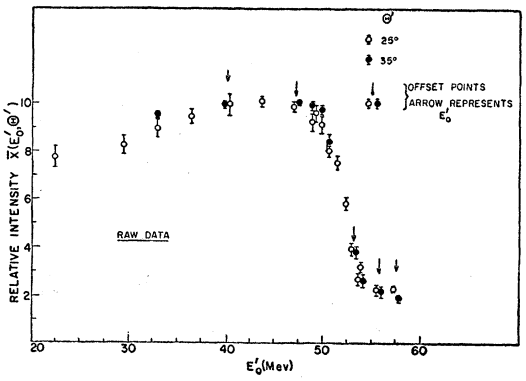

FIG. 5. Actual measured intensities as obtained for two spectrometer geometries with a solid 1-inch-diameter lithium target.

[14] Sagane, Dudziak, and Vedder, Bull. Am. Phys. Soc. Ser. II, 1, 174 (1956). See also reference 6 for a detailed discussion of these data.

[15] Sagane, Dudziak, and Vedder, Phys. Rev. 95, 863 (1954).

obtained with four variations of the spectrometer resolution—two of these were changes in target diameter and two of these were changes in the "angular slit" Θ' defined by the detector (see Appendix A). In these figures each point was obtained by combining the data from a series of measurements at each E_0' energy arising from frequent repeated changes of the magnetic field that covered the listed E_0' values for each spectrometer geometry. In the ratio method as many as forty resettings and remeasurements were made at one energy.

All our data are in accordance with Chauvenet's criterion for maximum acceptable deviations that occur in repeated measurements. A very small amount of our data ($<1\%$) was thrown out by this criterion. This amount is insignificant and would not influence the plotted data.

The results from each of the two tandem gates were analyzed and compared for possible systematic error resulting from the use of these gates. The two sets of data were in very good agreement (easily within the indicated statistics in these figures). Since these two sets of data are not independent, only one set of these results is used (actually the arithmetic mean is used).

In order to compare the Michel theory with experiment and determine the proper Michel parameter ρ_M, we must first modify Eq. (3) to incorporate the radiative corrections that have been omitted in the original derivation. It has been shown[3,4] that if one neglects the mass of the electron ($\epsilon=0$) in Eq. (3) and introduces these radiative corrections into the theory one obtains the following expression for the probable energy distribution of positrons resulting from an isotropic positive muon decay:

$$[P(\eta)]d\eta=(4/\tau_\mu)\eta^2[1+h(\eta,\Delta E)-\Lambda_1(\Delta E)]\times\{3(1-\eta)+\tfrac{2}{3}\rho_R[4\eta-3+\Lambda_1(\Delta E)\eta-3\Lambda_2(\Delta E)(1-\eta)]\}d\eta, \quad (4)$$

where ρ_R is related to the Michel parameter ρ_M by

$$\rho_R=\frac{\rho_M}{\{1+\Lambda_1(\Delta E)-\frac{2}{3}\rho_M[\Lambda_1(\Delta E)-\Lambda_2(\Delta E)]\}}. \quad (5)$$

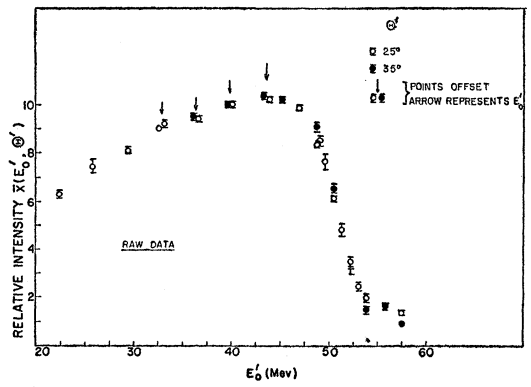

FIG. 6. Actual measured intensities as obtained for two spectrometer geometries with a solid $2\frac{3}{8}$-inch lithium target.

Here η is $p_e/p_{\max}$ (i.e., the fraction of maximum possible positron momentum), and ΔE is the acceptance-energy interval that is used in the experiment. The expression for $h(\eta,\Delta E)$ depends on the type of interaction that occurs between the particles during the disintegration process. For our calculations we have chosen the expression for vector coupling, which—to the accuracy of the calculations as given by Behrends *et al.*[3] and modified by Berman[4]—is also the expression for axial vector coupling. This expression is presented in Appendix C along with tabulated results for different values of ΔE. Found also in this Appendix are the defining expressions and numerical results of the integral functions $\Lambda_1(\Delta E)$ and $\Lambda_2(\Delta E)$. Since their values depend on the function $h(\eta,\Delta E)$ they also depend on the assumed coupling describing the nature of the interaction. As shown by the tabulated results, $h(\eta,\Delta E)$ and, to a lesser extent, $\Lambda_1(\Delta E)$ and $\Lambda_2(\Delta E)$ are varying functions of the energy interval ΔE that is used in the experiment.

Our procedure for determining the proper theoretical curves to be used for comparison with our measurements follows. Figures 16 and 17 in Appendix A illustrate two of our resolution functions. Each resolution function was subdivided into varying ΔE increments that correspond to the ΔE increments of the tabulated $h(\eta,\Delta E)$ functions. At a specific positron momentum η, the weight of each ΔE increment is given by $\omega(\Delta E,\eta)$, where

$$\int_0^{\Delta E_{\max}}\omega(\Delta E,\eta)d(\Delta E)=1.$$

We define the weighted functions

$$h(\eta,\langle\Delta E\rangle_{Av}),\quad \Lambda_1(\eta,\langle\Delta E\rangle_{Av}),\quad \text{and}\quad \Lambda_2(\eta,\langle\Delta E\rangle_{Av})$$

at a particular positron momentum η by

$$f(\eta,\langle\Delta E\rangle_{Av})=\int_0^{\Delta E_{\max}}f(\Delta E,\eta)\omega(\Delta E,\eta)d(\Delta E), \quad (6)$$

where $f(\eta,\Delta E)$ symbolizes one of these functions. These weighted functions were calculated for each η value. For each chosen Michel ρ_M parameter we used the weighted functions $\Lambda_1(\eta,\langle\Delta E\rangle_{Av})$ and $\Lambda_2(\eta,\langle\Delta E\rangle_{Av})$ to determine $\rho_R(\eta,\langle\Delta E\rangle_{Av})$ for each positron momentum η from Eq. (5). These weighted functions, $\rho_R(\eta,\langle\Delta E\rangle_{Av})$ and $h(\eta,\langle\Delta E\rangle_{Av})$, were then substituted into Eq. (4) to determine the proper value of the probability function $P(\eta,\rho_M)$ at each η value. In our calculations we used $\Delta\eta=0.01$ as our "mesh" (i.e., the interval between calculation values was 0.01). Following this procedure we constructed a family of theoretical curves for ρ_M (0.65 to 0.80), with ρ_M varying by 0.01 for each experimental geometry. In what follows, we refer to these curves as modified Michel curves.

For each geometry and each ρ_M value the expected measured intensity was obtained by folding the calcu-

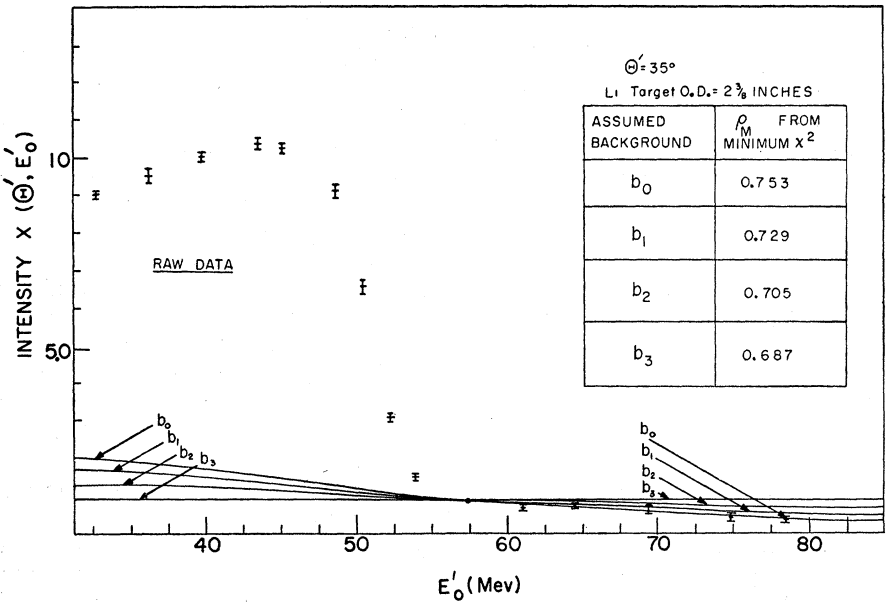

FIG. 7. Illustration of the serious effect on the Michel parameter of the subtracted background that arises from decay of muons in regions other than the desired spectrometer source.

lated resolution curve (Appendix A) that was obtained at each E_0' value into each one of this family of modified Michel curves. For these folding numerical calculations an 0.08-Mev mesh was used. In this way a table of expected theoretical intensities $P(E_0',\rho_M)$ *versus* values of ρ_M was calculated at each measured E_0' energy for each geometry of our spectrometer.

Prior to comparing these calculated intensities with the data shown in Figs. 5 and 6, one must subtract a background which could not be distinguished electronically by lifetime measurement from the true intensities arising from the target. The sources of this background are muons that decay from pions whose energies are sufficient for them to leave the target. These pions impinged on areas that could not be screened from the detector without destroying the experimental geometry. Since no intense pion beams were available at the time of this and another spectrometer experiment,[16] one had no choice but to tolerate and allow for this background due to energetic pions.

Knowledge of the nature of this background is imperative to a true prediction of the measured ρ_M parameter. The seriousness of this background is illustrated in Fig. 7 for one set of our data from the four geometries in our experiment. Here we replot the raw data shown in Fig. 6 which were measured with the $\Theta'=35°$ geometry. In addition we present experimental measurements above $E_0'=57.5$ Mev that are not included in Fig. 6. The point on this plot shown at $E_0'=57.5$ Mev is a very accurate measurement. At this magnetic setting our counting rate from the desired positron source (i.e., the lithium target) should be zero. [At a magnetic setting corresponding to $E_0'=56.5$ Mev the low-energy cutoff of the resolution function would be above 53.8 Mev (Fig. 17, Appendix A), and therefore no overlap is possible in the fold of this resolution function at $E_0'=57.5$ Mev with a modified Michel curve whose upper energy cutoff is about $E=52.8$ Mev.] Shown also on this plot are four background curves. One of these curves, indicated by b_0, is the background for this geometry as established by the methods described in Appendix D. The other three curves indicated by b_i ($i\neq 0$) are assumed background curves (positioned between b_0 and the assumed constant background b_3) and are used only to stress the influence of background subtraction on the ρ_M parameter. We tabulate in Fig. 7 the ρ_M values that result from the reduction of the data after background subtraction of the amount specified in

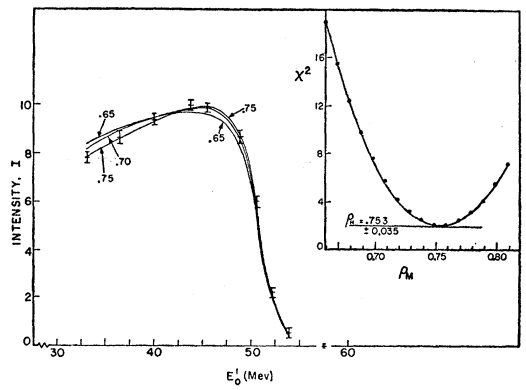

FIG. 8. Left: comparison of the reduced data for the stated spectrometer geometry (at $\Theta=35°$, $2\frac{3}{8}$-inch diameter lithium target) with three modified Michel curves that are normalized to the data by the minimum-χ^2 method. Right: plot of the dependence of the calculated minimum χ^2 on the Michel parameter.

[16] Crowe, Helm, and Taufest, Phys. Rev. **99**, 872 (1955); *Proceedings of the Sixth Annual Rochester Conference On High-Energy Nuclear Physics, 1956* (Interscience Publishers, Inc., New York, 1956).

each of the four cases. Realizing the seriousness of a wrong estimate of this background, we have arbitrarily assumed up to 50% more error in our established background in the lower energy region prior to the reduction of our most accurate measurements (Fig. 6).

In subtracting this background from the raw data (Figs. 5 and 6) we followed the same procedure for each of the four experimental geometries as is described in Appendix D. We present the results following this subtraction in Figs. 8, 9, and 10. In Fig. 10 the data from the two geometries involving the 1-inch lithium target are combined and treated as data from one experiment. As shown in detail in reference 6, we are justified in this decision by the fact that the errors are large and do not warrant a consideration of the small differences that exist in the resolution functions of these two geometries.

In the reduction of our data we found the χ^2 test a very suitable statistical method for determining what

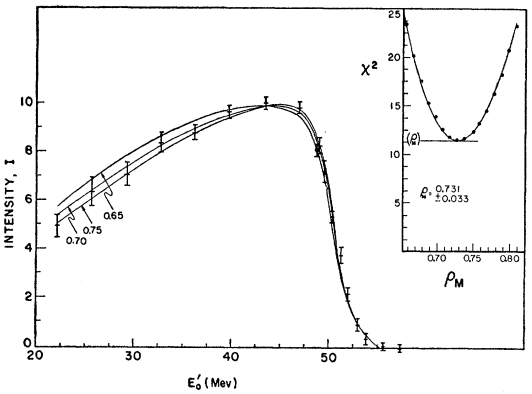

FIG. 9. Left: comparison of the reduced data for the stated spectrometer geometry (at $\Theta=25°$, $2\frac{3}{8}$-inch diameter lithium target) with three modified Michel curves that are normalized to the data by the minimum-χ^2 method. Right: plot of the dependence of the calculated minimum χ^2 on the Michel parameter.

member of the Michel family of curves agrees best with the measurements. As seen in Eq. (4), we are confronted with the problem of determining a particular Michel distribution that contains an unknown parameter[17] ρ_M about whose values we possess only such information as may be derived from our observations. We determine the proper Michel curve by solving for the most likely ρ_M parameter to render the expression

$$\chi^2=\sum_{E_0'}\sigma^{-2}(E_0')[I(E_0')-P(E_0',\rho_M)]^2 \qquad (7)$$

a minimum. We limit the sum to only those E_0' values

[17] Actually we should be dealing with the more general Eq. (3), following its modification for radiative corrections in muon decay, in which we would be confronted with the problem of determining two unknown parameters (ρ_M and ψ). Our simplification is valid under one of the following conditions: (a) when the parameter ψ is very close to 0 (it is zero in the two-component theory); (b) for $\psi=\pm1$, when the accuracy to which the parameter ρ_M is to be determined by the high-energy end of the spectrum (>30 Mev) is not in the neighborhood of 1 or 2%.

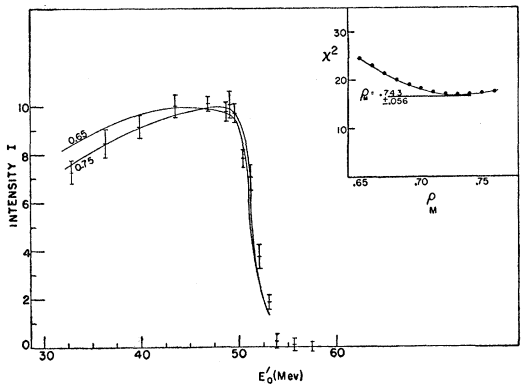

FIG. 10. Left: comparison of the reduced data (combined for $\Theta=25°$ and $\Theta=35°$, 1-inch-diameter lithium target) with two modified Michel curves that are normalized to the data by the minimum-χ^2 method. Right: plot of the dependence of the calculated minimum χ^2 on the Michel parameter.

whose measured intensities are greater than 2 on the ordinate scale of the reduced data (Figs. 8, 9, and 10), so as to avoid measurements that are greatly influenced by the magnitude of the subtracted background. In this equation $I(E_0')$ is the experimental intensity measurement at an E_0' setting, $\sigma(E_0')$ is the standard deviation of this measurement, and $P(E_0', \rho_M)$ is the corresponding predicted theoretical intensity for a specific ρ_M value.

Because of the experimental errors in the measured $I(E_0')$ intensities, some care is necessary in locating the proper normalization factor that fixes the ordinate scale of $I(E_0')$ in relation to the $P(E_0',\rho_M)$ scale before Eq. (7) can be used correctly in evaluating the χ^2 for a specific ρ_M value. In only a few of the many calculations presented in this paper was it found that normalization by area of the experimental measurements and the predicted measurements was correct. The proper normalization factor in our use of Eq. (7) was found by IBM-650 computer calculations, which were initiated by using an area normalization. This resulting χ^2 value was then compared with a newly determined χ^2 value based on a normalization factor that was slightly larger or smaller than the area normalization factor. By repetition of this hunting process a minimum χ^2 was determined at each ρ_M value. It is this minimum χ^2 that is plotted at each ρ_M value in Figs. 8, 9, and 10. We stress this point on normalization because, from our experience—even with as fine a ρ_M mesh ($\Delta\rho_M=0.01$) as is used in our calculations—a difference of 0.01 to 0.015 would have been introduced into the reported ρ_M value as determined by the minimum-χ^2 method by using only area normalization. (Our ρ_M value would have been lower.)

We summarize the results of these calculated minimum χ^2 values for each geometry in Figs. 8, 9, and 10. Shown also in these figures are the expected $P(E_0',\rho_M)$ values for $\rho_M=0.65$, 0.70, and 0.75, which have been normalized by the minimum-χ^2 method as discussed

TABLE IV. Summary of the measured ρ_M values.

Experiment	Spectrometer geometry: Lithium target diameter (inches)	Angular slit (degrees) Θ'	ρ_M	$\sigma_{\rho M}$
1	$2\frac{3}{8}$	35	0.753	0.035
2	$2\frac{3}{8}$	25	0.731	0.033
3	1	35	0.742	0.056
4	1	25		
Weighted mean value			0.741	0.022

above. For convenience the calculated $P(E_0',\rho_M)$ values at each ρ_M are connected by a continuous curve. Except at the measured E_0' values, these curves are not to be interpreted as obtained from IBM calculations. These curves, with Eq. (7), illustrate the energy region ($E_0'<50$ Mev) that is most significant in determining the final minimum χ^2 value.

We obtain the best value of ρ_M from the minimum χ^2 value of the plotted χ^2 calculations. This minimum is determined by setting equal to zero the first derivative with respect to ρ_M of a parabolic equation that is first obtained from a least-squares fit of the plotted χ^2 values. This best ρ_M value and its standard deviation as obtained from the data for the spectrometer geometry under consideration are also given in the respective figures. From the theory of propagation of errors we obtain, for the error on this ρ_M value,

$$\sigma_{\rho M}{}^2=\sum_{E_0'}\left(\frac{\partial\rho_M}{\partial I}\right)^2\sigma^2(E_0'), \tag{8}$$

which according to Eq. (7) may be expressed as

$$\sigma_{\rho M}{}^2=4\sum_{E_0'}\left[\left(\frac{\partial P}{\partial\rho_M}\right)^2-(I-P)\frac{\partial^2 P}{\partial\rho_M{}^2}\right]\left(\frac{\partial P}{\partial\rho_M}\right)^2\sigma^{-2}(E_0')$$

$$=4\sum_{E_0'}\left(\frac{\partial^2\chi^2}{\partial\rho_M{}^2}\right)^{-2}\left(\frac{\partial P}{\partial\rho_M}\right)^2\sigma^{-2}(E_0'). \tag{9}$$

It should be noted that the uncertainty contribution that results from the presence of the second Michel parameter [Eq. (3)] is not included in this expression for the error in the best ρ_M value.[17] In addition we omit the very small error that arises from the deviation (which is approximately 3%) of the χ^2 values as obtained from the parabolic equation from the plotted χ^2 values in the neighborhood of the minimum χ^2. Additional remarks concerning these data and the χ^2 test are given in reference 6.

Table IV summarizes the results of all experiments conducted in our measurements of the Michel ρ_M parameter. These results are dependent on the assumptions that were used, in particular on the background as estimated by methods described in Appendix D and on the assumption that the second Michel parameter ψ is 0.

MEASUREMENT OF THE MUON REST MASS

Another factor (other than background subtraction) that seriously effects the measurement of ρ_M is a misalignment of energy scale when the experimental intensities $I(E_0')$ are compared with the predicted intensities $P(E_0',\rho_M)$. A misalignment or an error of ± 0.25 Mev in W (i.e., a $\frac{1}{2}$% change in the absolute energy scale) yields a variation $\Delta\rho=\mp 0.03$ in ρ_M. Measurement of the magnetic field can determine the energy of the focused particle to sufficient precision to make the influence on ρ_M of the error in this energy very small. However, the question arises: To what accuracy can one determine the energy of the focused positron at the moment of muon decay, i.e., before it experiences ionization and radiation losses within the target? Because of the large effect of energy scale, one purpose of our experiment was to measure the maximum energy W by the same method as was used for the determination of the Michel parameter. This is indicated by the Type C experiment listed in Table II. As shown in Figs. 8 and 9, the separation of the different ρ_M curves is very small near the cutoff because of the steep slope that occurs in this positron energy region. The steepness of the slope for a set of Michel curves that are within a ρ_M interval of ± 0.05 is determined primarily by the resolution of the spectrometer. One may use this strong dependence of the shape of the positron spectrum on the spectrometer resolution to measure the value of W without knowing precisely the value of the Michel parameter ρ_M.

In our experiment we have used three different targets as the primary means of change in spectrometer resolution. For each of these three targets we determined the resolution of our spectrometer. Using the modified Michel equation that arises from Eq. (4) for $\rho_M=0.73$, we calculated the expected family of theoretical intensities for different W values and for each resolution by the folding procedure we previously described. If these calculations for each spectrometer resolution were plotted, they would represent a family

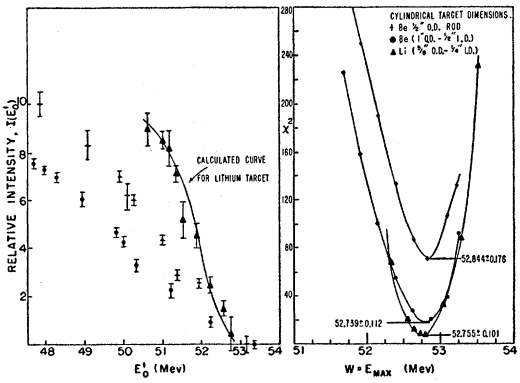

FIG. 11. Left: reduced experimental data as obtained for three different spectrometer resolutions in a study of the maximum positron energy. Right: plot of the dependence of the calculated minimum χ^2 on the maximum positron energy for each set of data.

of steeply varying curves, each indicating a different W cutoff energy.

The data from the three Type C experiments are presented in Fig. 11. The plotted data illustrate the strong effect of spectrometer resolution on the Michel spectrum near the maximum position energy. Because normalizations are involved in presenting these data on one plot, this illustration should be treated as qualitative. Each set of data is analyzed separately and we give quantitative significance only to this analysis.

We analyze each experimental set of measurements by the minimum-χ^2 method that we previously described. To do this we rewrite Eq. (7), after replacing ρ_M by W, so that we have

$$\chi^2=\sum_{E_0'}\sigma^{-2}(E_0')[I(E_0')-P(E_0',W)]^2. \quad (10)$$

As an illustration, a curve connecting the predicted calculated intensities at one W value, normalized by determination of the minimum χ^2 at this W value, is also plotted in Fig. 11 for one set of measurements (lithium target). The most probable value of W is determined from the minimum χ^2 obtained by setting equal to zero the first derivative of the fitted parabolic equation representing the calculated minimum χ^2 values as a function of W. To determine the standard error on this W measurement, we use the expression

$$\sigma_W{}^2=4\sum_{E_0'}\sigma^{-2}(E_0')\left(\frac{\partial P}{\partial W}\right)^2\left[\frac{\partial^2\chi^2}{\partial W^2}\right]^{-2}. \quad (11)$$

The results of our calculations are shown in Fig. 11 and are also summarized in Table V. The very high χ^2 values for the experiment using a Be target ($\frac{1}{2}$-inch diameter) are a direct result of the high measured intensity at $E_0'=52$ Mev.

Because these measurement have been made in air, a small energy correction is necessary in the energy scale to account for positron energy loss in air. (This correction was included in the energy scale of the previously discussed data.) To establish the most probable path length in air, we have used the data from our α-particle studies on the resolution of a spiral-orbit spectrometer. One phase of these studies involved positioning a well-collimated line source of monoenergetic α particles at a fixed radius and measuring the intensity and shape of the resolution at the detector by varying the magnetic field. The line source was rotated after each measurement (i.e., θ was varied and r_0 was constant) until measurements had been made for angles covering a complete 360° rotation of the line source. From these data an experimentally measured curve of collection probability as a function of angle of emission with respect to the α-particle detector was determined. Each angle of emission corresponds to a particular path length (Fig. 2). From these relations a most probable path of positrons in air was determined. Following the procedures outlined in Appendix A, we have calculated the most probable energy loss by using Sternheimer's results[18] for nitrogen and oxygen. These calculations yield an 0.11-Mev correction to the measured value of the maximum energy. Adding this correction to the weighted mean value appearing in Table V, we obtain $W=52.87\pm0.069$ Mev for the most probable value of the maximum positron energy.

TABLE V. Summary of the measured maximum positron energy W.

Experiment No.	Spectrometer target Element	External and internal diameters (inches)	W (Mev)	σ_W (Mev)
1	Li	($\frac{5}{8}$–$\frac{1}{4}$)	52.755	0.101
2	Be	$\frac{1}{2}$ (solid)	52.844	0.175
3	Be	(1–$\frac{1}{2}$)	52.739	0.112
Weighted mean value			52.763	0.069

A measurement of the maximum positron energy W is also a measure of the muon rest mass μ, because of the relation between these two quantities and the known electron mass ϵ, which is given by $W=(\mu^2+\epsilon^2)/2\mu$. From our value of W and this simple algebraic relation, we obtain $\mu=(206.94\pm0.27)\epsilon$ for the most probable muon rest mass.

STUDY OF THE EFFECT ON ρ_M OF SOME SYSTEMATIC ERRORS

A third factor that will influence the measured ρ_M value is the shape of the resolution function that is used in determining the predicted intensities $P(E_0',\rho_M)$. In Appendix A we discuss the procedure of calculating our resolution. We have found that had we simplified our calculations by separating the resolution into two parts —i.e., first taking into account the effect on the Michel curve of ionization and radiation losses in the target (Fig. 14) and then folding in the magnetic resolution of the spectrometer (Fig. 18)—we would have arrived at a different ρ_M value (lower by approximately 0.02). This method of separating the magnetic resolution from energy losses in the target in accounting for the resolution of the combined system is only an approximation. In our reduction we also used a third method of accounting for the resolution of the combined system that led essentially to the same results as the resolution derived in Appendix A.

In the course of these computation we also varied some of the parameters that affect the shape of the resolution function.

We present in Table VI a summary of our calculated results on how these variations influence the ρ_M value in our experiment. Column 1 specifies the modification that has been made, and Column 2 the corresponding $\Delta\rho$ value.

[18] R. M. Sternheimer, Phys. Rev. **103**, 511 (1956); **91**, 256 (1953).

TABLE VI. Effect of modifications in resolution function on the ρ_M parameter.

Type of modification in resolution function from that described in Appendix A	Effect on Michel parameter $\Delta\rho_M$	Additional comments
Separation of magnetic axis of symmetry from geometric axis of symmetry	± 0.0014	Brought about by misalignment of magnetic poles. We observed a 3/64-inch separation. Part of this may be attributable to our inability to know the exact location of the center of the small bismuth probe.
Misalignment of axis of cylindrical target and magnetic axis of symmetry	$\leqslant \pm 0.0014$	Axis aligned with surveyor's transit to within width of the cross hairs.
Radial misalignment of detector, either physical or simulated by nonuniformity in sensitivity across counter (5% sensitivity variation in our experiment). At most a $\pm\frac{1}{8}$-inch shift might be allowed.	∓ 0.004	A small physical radial displacement of our detector will not significantly change the shape of the resolution. However, it will introduce shift in the energy scale.
Effect of z focusing	-0.0018	We find that neglecting the effect of z focusing in our experiment is equivalent to an energy shift in the abscissa scale of 0.015 Mev.
Error in angular aperture of the detector system, $\pm 1°$	± 0.006	A 1° error corresponds to a $\frac{1}{2}$-inch error in the height at $r=19$ inches. This height was frequentiy checked, thus eliminating the probability of such an oversight.
Small variations of electron distribution in the target [i.e., changing the volume-weighting factor $W(r_0)$ in Eq. (25)]	$\leqslant \pm 0.004$	Such variations could be caused by nonuniformities in the proton beam, small errors in parameters that yield the Landau distribution.
Elimination of the Bethe and Heitler modification of the Landau distribution which introduces corrections for positron energy losses by radiation processes (Appendix A)	-0.011	Calculated to test sensitivity of ρ_M to small errors in the assumptions leading to this correction. Such errors would not influence our value.
Elimination of positron-source contribution from the outermost shell of the target. (Target subdivided into 15 shells. Considering the inner 14 shells only. See Appendix A.)	-0.021	This corresponds to approximately a 12% change in target volume. The value is used to estimate the influence of "flyback" effect. Over the measured range of positron energies the target variation because of the flyback effect was $<0.2\%$, leading to a possible error $\Delta\rho<0.001$.

The results from this experiment have yielded a meson mass value of $\mu=(206.94\pm0.27)\epsilon$, which is in very good agreement with the value obtained by other methods. If we accept the error on this mass value as an estimate of our knowledge of the true energy-scale alignment, then we must introduce an error into the Michel parameter of $\Delta\rho=\mp0.0084$.

If one combines statistically this error for energy-scale misalignment, an assumed 25% systematic error in normalization of the computed background ($\Delta\rho=\pm0.010$; see Appendix D), and the errors presented in Table VI with the error of $\rho_M=0.741\pm0.022$ that is obtained by the computer under optimized conditions, the result becomes $\rho_M=0.741\pm0.027$.

Estimate of the Mass of the Neutral Particles in Muon Decay

In one of his earlier articles on the spectrum of the secondary positrons from muon decay,[19] Michel has also considered the decay scheme

$$\mu^{\pm}\rightarrow\epsilon^{\pm}+\lambda+\nu,$$

where λ is a neutral particle of spin $\frac{1}{2}$ with a mass either nonvanishing or (more probably) zero. The question arises, can an estimate be made of the probable upper limit to the mass of λ? We employ a graphical method to make this estimate in Fig. 12 by using our measured value of the maximum positron energy W and the most accurate reported value of the muon mass that does not take our measurement into account.[20] In this case the maximum energy of the positron in muon decay is given by the expression

$$W=(\mu^2+\epsilon^2-\lambda^2)/2\mu,$$

where the assumption is made that the neutrino mass is zero. Shown in Fig. 12 is a family of curves for different values of the mass λ as given in electron mass units. Also plotted in this figure are two points: (a) our measured value of W against the most accurate quoted muon mass, $\mu=(206.86\pm0.11)\epsilon$, and (b) our value of W against the muon mass as determined from mesonic

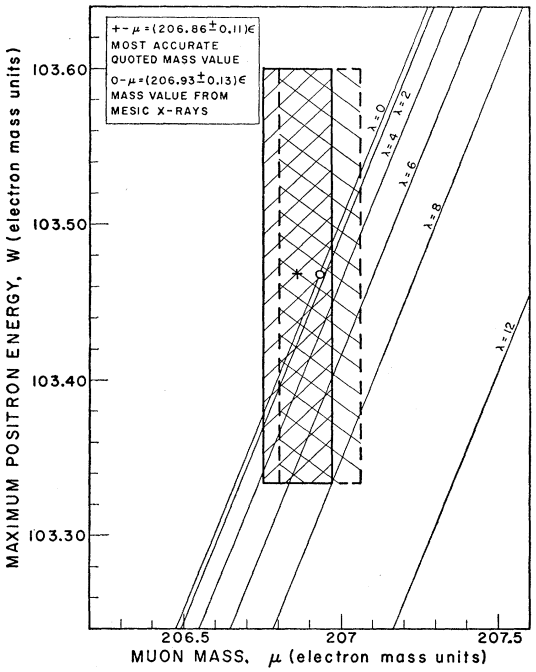

FIG. 12. Graphical estimate of the allowable neutral particle mass in positive muon decay. The hatched region is the area defined by the standard deviations in our measurement of W and the muon mass μ.

[19] L. Michel, Nature **163**, 959 (1949).

[20] Cohen, Crowe, and DuMond, *Fundamental Constants of Physics* (Interscience Publishers, Inc., New York, 1957).

x-rays, $\mu=(206.93\pm0.13)\epsilon$. Each of these points represents the center of a hatched region that defines the area subtended by the standard deviations of the measurements of W and μ. From examination of the figure, a probable upper limit to the mass of the neutral decay particle λ is obtained; it is 8 electron masses if the best value of the muon mass is used, and 9 electron masses if the muon mass as determined by mesonic x-rays is used.

ACKNOWLEDGMENTS

We should like to acknowledge the interest of Dr. Walter Barkas, and helpful discussions with numerous members of the physics staff during the course of this experiment. In particular we should like to express our gratitude to Dr. Alper Garren and Dr. Warren Heckrotte for their independent study of the resolution of our spectrometer during the earlier stages of the experiment. We should also like to acknowledge the invaluable help of Mr. Michael Lourie in the programing of the tedious computations on the IBM computer. Finally we should like to express our appreciation to Mr. James Vale and the entire cyclotron crew for efficient operation of the cyclotron during the experiment.

APPENDIX

A. Ionization and Straggling; Spectrometer Resolution

The resolution of the spectrometer was obtained by use of an IBM-650 computer and the following numerical calculations.

The radius of the cylindrical target was subdivided into fifteen equal segments. The circular boundaries of these radial segments defined a target volume. In what follows let r_0 represent the mean radius of any one of these fifteen cylindrical segments. For each radius r_0 a probability-of-occurrence function of a straight-line path length t through the target was determined. This probability-of-occurrence function results from a numerical calculation of the angle subtended by a path length t and $t+\Delta t$, where Δt was set equal to 0.005 inch. According to the procedure of Yang,[21] the most probable path length l for an electron was calculated from each straight-line path length t by use of the simplified expression $l=t(1+t/\lambda)$, where λ is the characteristic scattering length. We used the result as obtained by Scott[22] for the definition of λ, which is

$$\frac{1}{\lambda}=\frac{2\pi e^4Z^2N}{p^2v^2}\ln\left(\frac{150pc}{mc^2Z^{\frac{1}{3}}}\right), \tag{12}$$

where m, p, v, and e are the mass, momentum, velocity, and charge of the electron, c is the velocity of light, Ze is the charge of the scattering nucleus, and N is the number of nuclei per cm^3. This calculation yielded fifteen separate probability-of-occurrence functions $P(l,r_0)$ (one for each r_0) of the most probable path lengths for electrons originating in the cylindrical volume segment defined by a differential radial element at a radius r_0. (For example see Fig. 13.)

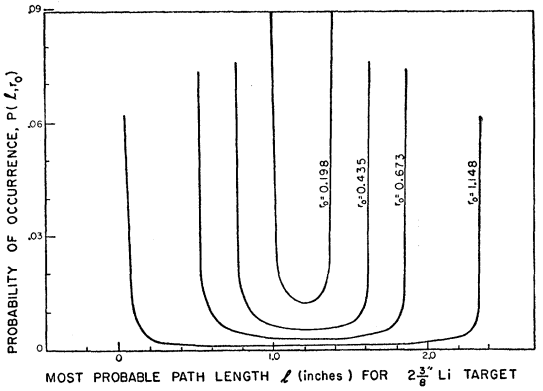

FIG. 13. Calculated probabilities of the most probable positron path length l in a solid cylindrical lithium target as a function of target radius r_0.

A monoenergetic beam of electrons of energy E_0, after traveling a certain path length l in material, loses energy by ionization and radiation processes. The probable energy distribution of an initially monoenergetic electron beam that results from collision losses after it has traveled a path length l through matter has been calculated approximately by Landau[23] and more recently by Shultz,[24] Blunck and Leisegang,[25] and Symon.[26] We find that the analytic expression given by Blunck and Leisegang for this energy distribution would be very useful in our type of calculation. However, calculations reveal that the full width at half height of the energy-distribution function that is obtained by use of their results is smaller by 7% than that given by Symon. Since Symon's results are in excellent agreement with the experimental data of Goldwasser, Mills, and Hanson,[27] we have used his data to represent what is normally referred to as the Landau distribution in our work. In addition we have extended the tail of Symon's calculated probability distribution from abscissa values $(\Delta-\epsilon_p)/\Delta_0=10$ to $(\Delta-\epsilon_p)/\Delta_0=15$ by Landau's derived inverse-square behavior for this region.

For an initial electron energy E_0 associated with each electron path length l (cm) there is a probable electron-energy (or Landau) distribution $L(l,\Delta)$ and also a most probable electron energy loss ϵ_p. The most probable energy loss ϵ_p was obtained by using the Sternheimer

[21] C. N. Yang, Phys. Rev. **84**, 599 (1951).
[22] W. T. Scott, Phys. Rev. **76**, 213 (1949).
[23] L. Landau, J. Phys. (U.S.S.R.) **8**, 201 (1944).
[24] W. Shultz, Z. Physik **129**, 530 (1951).
[25] O. Blunck and S. Leisegang, Z. Physik **128**, 500 (1950).
[26] Keith R. Symon, thesis, Harvard University, 1948 (unpublished).
[27] Goldwasser, Mills, and Hanson, Phys. Rev. **88**, 1137 (1952).

expression,[18]

$$\epsilon_p=\frac{2\pi NZe^4}{mv^2}l\left[\ln\frac{2mv^2(2\pi NZe^4l/mv^2)}{I^2(1-\beta^2)}-\beta^2+0.37-\delta\right], \quad (13)$$

which can also be written as

$$\epsilon_p=\Delta_0\left[B+1.06+2\ln\frac{p}{mc}+\ln\frac{A\rho' l}{\beta^2}-\beta^2-\delta\right],$$

where $\Delta_0=A\rho' l/\beta^2$, and where ρ' is the density of target material (g/cm^3), A and B are tabulated constants as presented in (21a), and δ is given approximately by an analytic expression. For lithium we used

$$\delta=4.606X-3.07+0.374(2-X)^{3.05}, \quad (\text{for } X<2)$$
$$\delta=4.606X-3.07, \quad (\text{for } X>2) \quad (14)$$
$$X=\log_{10}(p/mc).$$

In addition the electron loses energy by radiation in passing through matter. To take account of this radiation correction we use the results of Bethe and Heitler[28] to modify each Landau distribution in the following manner. Consider each ordinate $L_i(l,\Delta_i)$ of a normalized Landau probability distribution,

$$\int_{E_0}^{0} L(l,\Delta)d\Delta=1,$$

that results only from ionization losses, for a monoenergetic electron beam of energy E_0 traversing matter and having the most probable electron path length l. We have $\Delta_i=(E_0-E_i)$, which represents the corresponding electron energy loss due to ionization only. Each ordinate $L_i(l,\Delta_i)$ must first be modified by $W(l,E_i)$, i.e., by the probability that an electron still has approximately the energy E_i after radiation losses are also considered. To calculate $W(l,E_i)$, we use the Bethe-Heitler relation

$$W(bl,y)=[bl-1,y]!/\Gamma(bl), \quad (15)$$

i.e., the probability that an electron still has an energy greater than e^{-y} times the energy E_i after traversing the path length l. The $(bl-1,y)!$ is the "incomplete gamma function,"[29] $y=\ln[E_i/(E_i-k)]$; k is the energy loss by radiation after traversing a short distance; and b is a constant whose value depends on the density and nuclear charge of matter being considered. For lithium, b is 5.56×10^{-3} cm^{-1}. To determine $W(l,E_i)$, we set $k=k'=1.28$ kev.

In addition, the Landau probability-distribution ordinates are modified by contributions from those electrons that experience radiation losses, i.e., $[1-W(l,E_i)]\times L_i(l,\Delta_i)$. Because of radiation losses there is a shift of electrons from the higher E_i energies to lower electron energies, resulting in an increase of the $W(l,E_i)L_i(l,\Delta_i)$ probability ordinates for lower E_i energies. To determine $\delta L_j(l,E_j)$ (that is, the amount of this increase in a particular probability ordinate that corresponds to an energy E_j), we use the expression

$$\delta L_j(l,E_j)\cong\sum_i[1-W(l,E_i)]\Delta w(y_{ij})L_i(l,\Delta_i), \quad (16)$$

where the summation over i is the contribution of all electron energies $E_i>E_j$, and y_{ij} is the value of y obtained for a particular energy loss through radiation $k_{ij}=(E_i-E_j)$. For $w(y)$ we use the Bethe-Heitler expression

$$w(y)=\exp(-y)y^{(bl-1)}/\Gamma(bl), \quad (17)$$

which represents the probability that the energy of an electron that has traversed a finite distance l has decreased by the factor e^{-y}. In all our calculations we normalize by setting $w(y)=100\%$ for $k=k'=1.28$ kev. $\Delta w(y_{ij})$ is defined as the difference between two values of $w(y)$ evaluated for $k=E_i-E_j$ (in Mev) and $k=(E_i-E_j-0.00128)$. (In these calculations we use a fixed energy mesh of 0.04 Mev.)

The Landau probability ordinates, modified to take into account electron radiation losses, are given by the sum $[W(l,E_j)L(l,E_j)+\delta L_j(l,E_j)]$ for each most probable path length l and initial electron energy E_0. In addition, this sum must be multiplied by the probability of occurrence, $P(l,r_0)$, of the path length l for the differential volume segment designated by r_0. Four of the fifteen probability functions $P(l,r_0)$ are illustrated in Fig. 13. These are normalized so that we have

$$\int_{l_{\min}}^{l_{\max}} P(l,r_0)dl=1.$$

For obtaining the most probable electron distribution $Q(\Delta,r_0)$ from a differential volume r_0 that results from a monoenergetic electron source the above calculations are performed for each possible l value. The resulting sum of the contributions from all l values yields the desired probability,

$$Q(\Delta,r_0)=\int_{l_{\min}}^{l_{\max}}[W(l,k)L(l,\Delta)+\delta L(l,\Delta)]P(l,r_0)dl. \quad (18)$$

We evaluated this expression for each r_0 by approximating the integral by a sum. For the innermost first six r_0 shells a Δl mesh of 0.2 mm was used. A Δl mesh of 0.4 mm was used for the seventh, eighth, and ninth shells and 0.5-mm Δl mesh for the remaining larger r_0 shells.

Figure 14 illustrates the function $Q(\Delta,r_0)$ for five of the fifteen different r_0 values for a lithium cylindrical target whose diameter is 2.375 inches. These $Q(\Delta,r_0)$ values represent the most probable energy distribution for electrons initially at 50 Mev, originating at a

[28] H. Bethe and W. Heitler, Proc. Roy. Soc. (London) **A146**, 83 (1934); W. Heitler, *Quantum Theory of Radiation* (Oxford University Press, London, 1954), p. 379.

[29] K. Pearson, *Tables of the Incomplete Γ-Function* (Cambridge University Press, Cambridge, 1946).

specific target position r_0, and undergoing ionization and radiation losses while emerging from the target. The areas under these curves are normalized so that we have

$$\int_{\Delta_{min}}^{\Delta_{max}} Q(\Delta,r_0)d\Delta=1.$$

Consider now the magnetic focusing of these electrons when the source is centrally located in a magnetic field such that the longitudinal axis of the cylinder coincides with the magnetic axis of a spiral-orbit spectrometer. Suppose that this is the z axis of a cylindrical coordinate system (r,θ,z) and that $z=0$ defines the median plane of the spectrometer. One of the principal spectrometer requirements is that the magnetic field be axially symmetric, that is, in a cylindrical coordinate system,

$$\begin{aligned} B_r(r,z)&=-B_r(-z,r);\\ B_\theta&=0;\\ B_z(r,z)&=B_z(r,-z). \end{aligned} \tag{19}$$

As illustrated in Fig. 2, equations of motion show that a charged particle originating in the cylindrical source spirals into an orbit $r=\rho$ about the z axis if the magnetic conditions are such that its radial velocity and radial acceleration become zero. For motion in the median plane, these requirements state[7–12] that the vector potential is at a maximum at $r=\rho$ and that the following relations exist between the vector potential, magnetic field, and radius $(r=\rho)$ of the circle of convergence at $r=\rho$:

$$A(\rho)=\rho B(\rho)=\frac{1}{\rho}\int^{\rho} rB(r)dr. \tag{20}$$

It was first pointed out by Iwata, Miyamoto, and Kotani[8] that this expression defines a circle of convergence and that the radius ρ of this circle depends on the shape of the magnetic field strength irrespective of the absolute value of the magnetic field. Figure 4 presents the shape [with respect to strength $B(r)$] of the radial magnetic field that was used in this experiment. It also illustrates a graphical method that can be used to determine the value of the radius ρ.

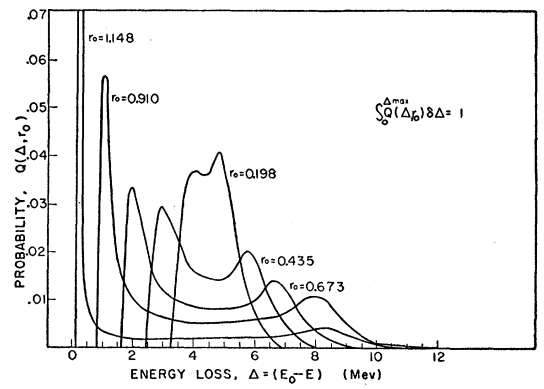

FIG. 14. Calculated radial dependence of the probabilities of positron-energy loss for a monoenergetic positron source undergoing combined ionization and radiation energy losses in emerging from a solid cylindrical lithium target.

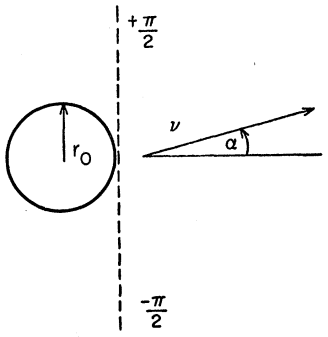

FIG. 15. A source represented by a cylindrical shell of radius r_0 located concentric with the axis of magnetic symmetry in a spiral-orbit spectrometer.

Suppose that a detector is located so that the center of the detector coincides with the circle of convergence and so that the radial dimension of this detector defines two circles, in the neighborhood of the circle of convergence, having radii equal to $\rho+d$ and $\rho-d$. Particles whose spiral paths pass through the inner circle can be detected. The probability of detection for these particles varies between zero and one. It depends on the length of the spiral path within the annular region defined by the two circles of radii $\rho+d$ and $\rho-d$. This portion of the path length can best be measured by the central angle Θ that it subtends. For all practical purposes the detection probability is unity for all particles whose paths are within these radial boundaries and whose central angles are $\gtrsim 2\pi$, since these are lost after passing through the detector for the first time.

Consider now a monoenergetic source located concentric to the axis of magnetic symmetry at a radius r_0 as illustrated in Fig. 15. Suppose that the source intensity is independent of the angle of emission α. Under these conditions it can be shown[7–12] that to a very good approximation the subtended central angle is given by

$$\begin{aligned} &\Theta\simeq\kappa\sqrt{2}\,\cosh^{-1}(\mu+\epsilon\sin\alpha)^{-0.5}\\ &\qquad\text{for}\quad(\mu+\epsilon\sin\alpha)>0,\quad\text{(Case 1)}\\ &\Theta\simeq\kappa\sqrt{2}\,\sinh^{-1}(|\mu+\epsilon\sin\alpha|)^{-0.5}\\ &\qquad\text{for}\quad(\mu+\epsilon\sin\alpha)<0,\quad\text{(Case 2)} \end{aligned} \tag{21}$$

where κ is a constant, obtained from the shape of the magnetic field at the focus orbit, that is related to the more familiar field parameter $n=-(r/B)(dB/dr)$ by the expression $\kappa=[2(n-1)]^{\frac{1}{2}}$,

$$\mu=\kappa^2\frac{\Delta B}{B}\frac{\rho^2}{d^2}, \tag{22a}$$

$$\epsilon=\kappa^2\frac{r_0}{\rho}\frac{\rho^2}{d^2}, \tag{22b}$$

Case 1 represents all particles that do not have sufficient

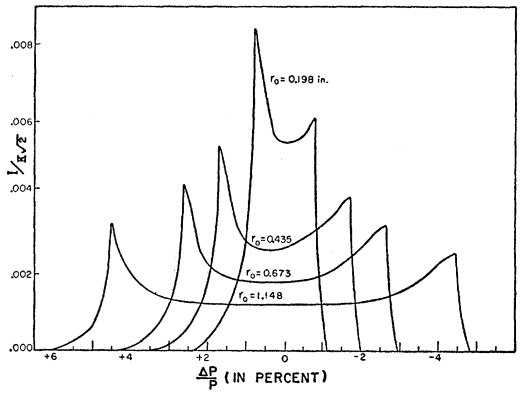

FIG. 16. Dependence of resolution on parameters of a spiral-orbit spectrometer (expressed in terms of momentum) $\Theta=35°$, $\kappa=0.90$, $2\frac{3}{8}$-in. Li target.

momenta to escape from the region of the magnetic field. Case 2 applies to all particles whose momenta are such that they can escape from this region.

The resolution of a homogeneous monochromatic source located at r_0 is given by the integral of Θ for all possible values of α. In an experiment a detector and a slit system located so that the defining edge is at a radius $r=\rho-d$ subtended a central angle Θ'. This angular width Θ' of the detecting system limits the actual number of detectable particles as given by Θ. For such a system the resolution of the spectrometer is given by

$$I(\mu,\epsilon,\Theta')=\frac{1}{2\pi^2}\int_{-\pi/2}^{\pi/2}(\Theta-\Theta')d\alpha, \quad \text{for} \quad \Theta\geqslant\Theta', \quad (23)$$

and

$$I(\mu,\epsilon,\Theta')=0, \quad \text{for} \quad \Theta<\Theta'.$$

In our experiment Θ' had two values, $\Theta'=25°$ and $\Theta'=35°$. We have numerically evaluated these integrals for the two values of Θ' by the following simplified procedure. Given Θ', μ, and ϵ, we used Simpson's $\frac{1}{3}$ rule with a $\Delta\alpha$ mesh of 1 degree. As previously mentioned, proper care was taken in evaluating the region $2\pi\leqslant\Theta\leqslant\infty$.

Figure 16 illustrates the intensity-distribution function $I(\mu,\epsilon,\Theta')/\kappa\sqrt{2}$ for four of the fifteen different r_0 or ϵ values as obtained for $\kappa=0.90$ and $\Theta'=35°$. For each r_0 the total momentum width of the intensity distribution is limited by the angular width Θ' and can be calculated from the expression

$$-[\epsilon+\operatorname{csch}^2(\Theta'/\kappa\sqrt{2})]\leqslant\mu\leqslant[\epsilon+\operatorname{sech}^2(\Theta'/\kappa\sqrt{2})]. \quad (24)$$

These calculations are for trajectories in the median plane. They are applicable only to such trajectories and to those that closely approximate this motion. Therefore cylindrical copper electron stoppers (2 in. thick and 30 in. i.d.) were used to limit the aperture above and below the median plane to $z=\pm1.5$ in. These are shown in Fig. 1. This limitation of aperture, plus the fact that the magnetic field strength is very flat (up to $r=15$ inches), permits us to use these curves as good approximations for the magnetic focusing properties of the spectrometer. We have verified this experimentally by studies with monoenergetic alpha particles (and will present these results in a forthcoming paper) and also by calculations (Table VI).

Having determined the Q and I distribution functions, we can now calculate the function $R(E_0',\Theta',E)$, which represents the spectrometer resolution for electrons that are initially born in a cylindrical target with an energy E, lose energy by radiation and ionization, and are brought to a focus at the detector of angular width Θ' by a magnetic field strength set so that the value of the vector potential at the focus orbit is a measure of an electron energy E_0'. We obtain $R(E_0',\Theta',E)$ by a series of numerical calculations whereby we approximate the integral over r in the expression

$$R(E_0',\Theta',E_0)=\int_0^{r_{\max}}F(E_0',E_0,\Theta',r_0)W(r_0)dr_0$$

$$=\int_0^{r_{\max}}W(r_0)dr_0\int_0^{E_0}I(E_0',\Delta E',\Theta',r_0)\times Q(E_0\Delta E,r_0)dE \quad (25)$$

by a summation of fifteen different r_0 shells. Here $W(r_0)$ is the volume-weighting factor. The integral determining the function F is approximated by numerical calculations, in which 0.04 Mev is used as a ΔE mesh for each E_0 value. Neighboring E_0 values differ by 0.08 Mev.

Figures 17 and 18 summarize the results of these calculations for two different geometries that were used in this study of the Michel ρ_M parameter. (For additional details and resolutions of the other geometries see reference 6.) These are the resolution curves that were used when the magnetic field strength was such that the focus-orbit positron energy E_0' was 50 Mev. Therefore they represent the resolutions of our spectrometer for the specified geometries near the maximum positron

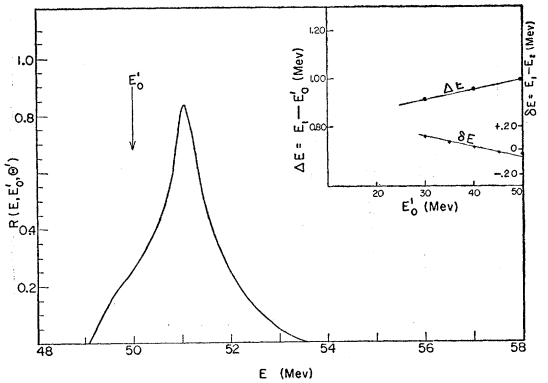

FIG. 17. Combined resolution for positrons having a focus energy of 50 Mev for $\Theta=35°$, $\kappa=0.90$, 1-in. Li target.

energy that is possible in the muon decay. Also shown are the variations with magnetic setting of the focus-orbit energy E_0' and the energy E_2 of the peak of the resolution, from the energy E_1 at which the half area of the resolution occurs. These illustrate the point that the simple magnetic-spectrometer property ($\Delta P/P$ equals a constant) no longer holds. This arises from the fact that positron ionization and radiation losses do not have the same momentum dependence as the magnetic-focusing properties of the spectrometer.

Figure 19 presents a summary of additional calculations illustrating the focusing properties of the spiral-orbit spectrometer when straggling, ionization, and radiation losses are neglected. We define the resolution $R(\Delta P/P,\Theta')$ by the integral

$$R(\Delta P/P,\Theta')=\int_0^{r_{\max}} I(\Delta P/P,\Theta',r_0)W(r_0)dr_0. \quad (26)$$

The plotted curves are for the four geometries stated. They are the results of numerical calculations in which we approximate the integral over r by a summation of fifteen different r_0 shells. Here $W(r_0)$ is the volume-weighting factor.

As a final remark we would like to state that errors exist in some of the published resolution curves in reference 8.

B. Effect of Saturation on the Michel ϱ_M Parameter

One point that has not been stressed is the effect of small changes of the magnetic-field distribution on the counting rate. As has been stated, one determines the position of the focus orbit from the solution of Eq. (20). In our early experiments, which led to publication of our preliminary evaluation of the Michel parameter,[15] we compared the positions of this focus orbit obtained from two magnetic distributions. The radii of these two positions were $\rho=27.13$ inches and $\rho=26.93$ inches. Since the radial dimension of our detectors was 3 inches, we did not attribute any significance to this difference,

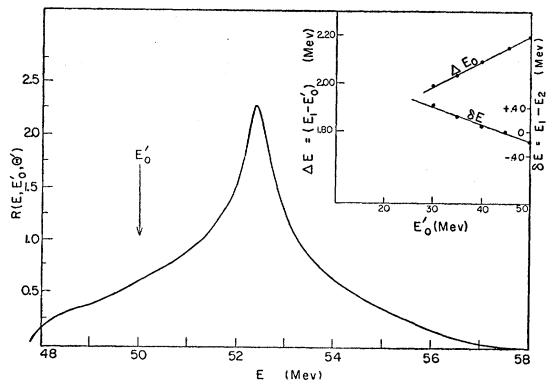

FIG. 18. Combined resolution for positrons having a focus energy of 50 Mev for $\Theta=35°$, $\kappa=0.90$, $2\frac{3}{8}$-in. Li target.

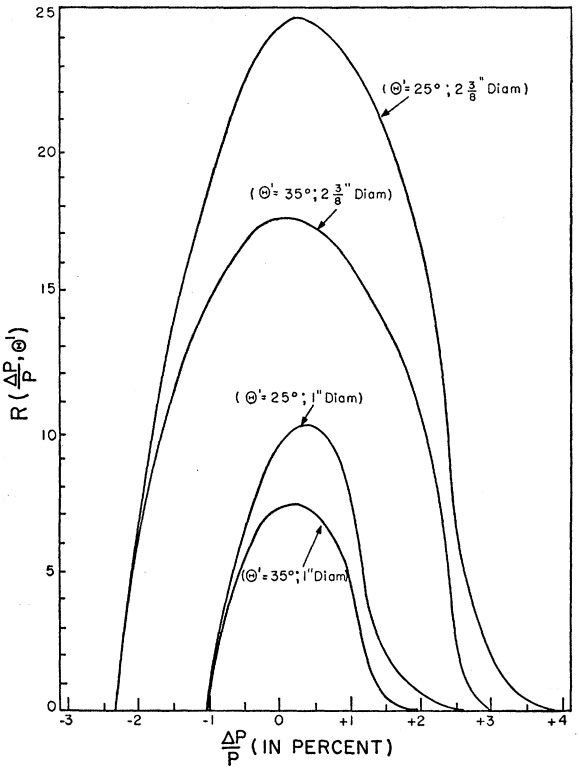

FIG. 19. Comparison of spiral-orbit spectrometer resolution for the four experimental geometries.

which corresponds to a 0.7% difference in momentum at the position of focus and is even less when the arithmetic average of these two values is used.

The true significance of this difference was finally recognized when the large pole tips that were part of a large vacuum chamber (Fig. 4) were removed and the spectrum remeasured with poles that were the core of the magnet (Fig. 4). Because of the striking difference in the shapes of our measured positron spectrum obtained with the two magnetic geometries, magnetic-field distributions were measured at numerous positron energies (for method, see Fig. 2). From these magnetic measurements it was learned that there was a systematic decrease of the focus-orbit position in the old magnetic geometry, and that this decrease resulted from a gradual change of the shape of the radial magnet field distribution. This is partially summarized in Table VII, where $B_{\max}$ is the maximum magnetic field in the median plane (which for this geometry occurs at $r=5$ inches), $A(\rho)$ is the vector potential at the focus orbit, ρ is the radial position of the focus orbit, and the $B_r/B_{\max}$ are the ratios of the magnetic field at the stated radii to the maximum magnetic field. For the radial magnetic-field distribution to be the same, the ratios in each of the five $B_r/B_{\max}$ columns should be the same. Because the slit system remains fixed for each Θ' geometry, the decrease in the focus orbit together with the changing of the radial magnetic-field distribution constitutes an

TABLE VII. Summary of saturation-effects study of the old[a] geometry. E_0', B_{max}, $A(\rho)$, ρ, and the ratio B_r/B_{max} are defined in the text.

E_0' (Mev)	B_{max} $r=5.0$ in. (gauss)	$A(\rho)$ (kilogauss-in.)	ρ (in.)	Ratio B_r/B_{max} $r=11.25$ in.	$r=18.25$ in.	$r=23.0$ in.	$r=25.0$ in.	$r=27.0$ in.
45.36	7021	59.57	27.32	0.874	0.634	0.451	0.389	0.322
47.59	7403	62.50	27.13	0.873	0.632	0.446	0.383	0.316
48.74	7593			0.873	0.631	0.443	0.380	0.313
49.82	7772			0.873	0.630	0.441	0.378	0.313
50.90	7949	66.84	29.63	0.873	0.629	0.440	0.376	0.310
51.79	8101	68.01	26.86	0.874	0.628	0.438	0.374	0.307
52.79	8273	69.32	26.81	0.874	0.628	0.436	0.372	0.305
	8453			0.874	0.627	0.434	0.369	0.303
						Repeated measurements		
45.47	7028	59.72	27.33					
52.19	8185	68.53	26.89					

[a] See reference 15.

increase in resolution as positron energy is increased. This additional change in resolution caused the striking change in counting intensity that we overlooked in reporting our earlier data.[15]

Table VIII represents similar information on the new magnetic geometry that was used throughout this experiment. From this table the conclusion can be drawn that the necessary condition—that the shape of the magnetic field distribution remain the same over the positron-energy range of this experiment— has been fulfilled by our new geometry.

In addition to making these magnetic-distribution studies, we made another study in which we employed a scattered positron beam created by photons from a 330-Mev synchrotron to determine the influence of saturation on ρ_M. Details of this study are summarized in reference 6.

C. Radiation Corrections to Muon-Decay Spectrum

Berman has recalculated the electromagnetic interactions that constitute the radiative correction to the muon decay.[4] His results differ from those of Behrends, Finkelstein, and Sirlin (BFS)[3] because of an apparent use of an inconsistent method by the original authors for handling the infrared divergences, which arise separately in the real and virtual processes. The disagreement between the old and the new functions $h(\eta,\Delta E)$, $\Lambda_1(\Delta E)$, and $\Lambda_2(\Delta E)$ is significant. The difference between the old and the new exists in the function $X(\eta,\Delta E)$, which replaces the old function $V(\eta,\Delta E)$. This difference is given by

$$(X-V)=\{1-\tfrac{1}{6}\pi^2+\ln(\eta+w-1)[2\ln 2-w-\ln\eta]\}, \quad (27)$$

where $\eta=p_e/p_{max}$, i.e., the fraction of maximum possible positron momentum.

For the function $h(\eta,\Delta E)$ we used the expression for vector and axial vector coupling:

$$h_{V,A}(\eta,\Delta E)=\frac{\alpha}{2\pi}\left\{2(U+X)+\frac{6(1-\eta)}{(3-2\eta)}\ln\eta-4+\frac{(1-\eta)}{3\eta(3-2\eta)}\times\left[\left(\frac{5}{\eta}+17-34\eta\right)(\ln\eta+w)+34\eta-22\right]\right\}, \quad (28)$$

where

$$(U+X)=\left\{2\sum_{m=1}^{\infty}\frac{\eta^m}{m^2}-\frac{\pi^2}{3}+\ln\eta\left[\ln\left(\frac{1}{\eta}-1\right)-2w\right]+\frac{5w}{2}-w^2+(w-\ln\eta)(\ln+w-1)+\left(2\ln\eta+2w-1-\frac{1}{\eta}\right)\times\ln\left(1-\eta+\frac{2\Delta E}{m_1e}\right)\right\}. \quad (29)$$

Here we have $\alpha=1/137$, $w=\ln(m_1/m_2)=5.3327$, $m_1=$ rest

TABLE VIII. Summary of saturation-effects study of the new geometry.

E_0' (Mev)	B_{max} (gauss) $r=8$	$A(\rho)$ (kilogauss-in.)	ρ (in.)	Ratio B_r/B_{max} $r=16.0$ in.	$r=21.0$ in.	$r=23.0$ in.	$r=25.0$ in.	$r=26.0$ in.
30.34	3994	39.86	25.57					
48.64	6403	63.58	25.60	0.919	0.668	0.541	0.422	0.369
50.95	6703	66.91	25.59	0.920	0.669	0.542	0.422	0.371
52.49	6905	68.94	25.58	0.917	0.668	0.540	0.421	0.369
66.23	8762	86.98	25.56	0.917	0.667	0.540	0.420	0.368
76.08	10064	99.92	25.58	0.916	0.666	0.538	0.421	0.367

TABLE IX. Values of $h(\eta,\Delta E)$ as a function of ΔE [ΔE (in electron rest-mass units)].

η	0	$\frac{1}{4}$	$\frac{1}{2}$	1	2	3	4	5	6	7	8	9	10	12	16	20
0.01	4.5600	4.5598	4.5596	4.5592	5.5584	4.5576	4.5567	4.5559	4.5551	4.5543	4.5535	4.5527	4.5519	4.5503	4.5471	4.5440
0.03	1.3535	1.3534	1.3534	1.3532	1.3530	1.3527	1.3525	1.3522	1.3520	1.3517	1.3514	1.3512	1.3509	1.3504	1.3494	1.3485
0.05	0.6597	0.6596	0.6596	0.6595	0.6594	0.6592	0.6591	0.6590	0.6588	0.6587	0.6586	0.6584	0.6583	0.6580	0.6575	0.6569
0.08	0.3378	0.3378	0.3377	0.3377	0.3376	0.3376	0.3375	0.3374	0.3374	0.3373	0.3372	0.3371	0.3371	0.3369	0.3367	0.3364
0.10	0.2472	0.2472	0.2471	0.2471	0.2471	0.2470	0.2470	0.2469	0.2469	0.2468	0.2468	0.2468	0.2467	0.2466	0.2465	0.2463
0.13	0.1725	0.1725	0.1725	0.1725	0.1725	0.1725	0.1724	0.1724	0.1724	0.1724	0.1724	0.1724	0.1723	0.1723	0.1722	0.1721
0.15	0.1423	0.1423	0.1423	0.1423	0.1423	0.1423	0.1423	0.1423	0.1423	0.1422	0.1422	0.1422	0.1422	0.1422	0.1422	0.1422
0.18	0.1116	0.1116	0.1116	0.1116	0.1116	0.1116	0.1116	0.1116	0.1116	0.1117	0.1117	0.1117	0.1117	0.1117	0.1117	0.1118
0.20	0.09703	0.09703	0.09704	0.09704	0.09706	0.09708	0.09709	0.09710	0.09712	0.09713	0.09715	0.09716	0.09718	0.09720	0.09726	0.09732
0.23	0.08046	0.08047	0.08047	0.08049	0.08051	0.08054	0.08056	0.08059	0.08061	0.08064	0.08066	0.08068	0.08071	0.08076	0.08085	0.08095
0.25	0.07182	0.07183	0.07183	0.07185	0.07188	0.07191	0.07194	0.07198	0.07201	0.07204	0.07207	0.07210	0.07213	0.07219	0.07231	0.07243
0.28	0.06128	0.06129	0.06130	0.06132	0.06136	0.06140	0.06144	0.06148	0.06152	0.06156	0.06160	0.06164	0.06168	0.06175	0.06191	0.06206
0.30	0.05544	0.05545	0.05546	0.05548	0.05553	0.05557	0.05562	0.05566	0.05571	0.05575	0.05580	0.05584	0.05589	0.05598	0.05615	0.05632
0.33	0.04795	0.04796	0.04798	0.04800	0.04806	0.04811	0.04816	0.04822	0.04827	0.04832	0.04838	0.04843	0.04848	0.04858	0.04878	0.04898
0.35	0.04361	0.04362	0.04364	0.04367	0.04373	0.04379	0.04385	0.04390	0.04396	0.04402	0.04408	0.04414	0.04419	0.04430	0.04453	0.04474
0.38	0.03784	0.03786	0.03788	0.03791	0.03798	0.03804	0.03811	0.03818	0.03824	0.03831	0.03837	0.03844	0.03850	0.03863	0.03888	0.03913
0.40	0.03439	0.03441	0.03442	0.03446	0.03453	0.03461	0.03468	0.03475	0.03482	0.03489	0.03496	0.03503	0.03510	0.03524	0.03551	0.03578
0.43	0.02966	0.02968	0.02970	0.02974	0.02983	0.02991	0.02999	0.03007	0.03014	0.03022	0.03030	0.03038	0.03046	0.03061	0.03091	0.03121
0.45	0.02676	0.02678	0.02680	0.02685	0.02693	0.02702	0.02710	0.02719	0.02728	0.02736	0.02744	0.02753	0.02761	0.02777	0.02810	0.02841
0.48	0.02269	0.02272	0.02274	0.02279	0.02288	0.02298	0.02307	0.02317	0.02326	0.02336	0.02345	0.02354	0.02363	0.02381	0.02416	0.02451
0.50	0.02014	0.02016	0.02019	0.02024	0.02034	0.02044	0.02054	0.02064	0.02074	0.02084	0.02094	0.02104	0.02114	0.02133	0.02171	0.02208
0.53	0.01649	0.01652	0.01654	0.01660	0.01671	0.01683	0.01694	0.01705	0.01716	0.01727	0.01738	0.01748	0.01759	0.01780	0.01822	0.01862
0.55	0.01415	0.01418	0.01421	0.01427	0.01440	0.01452	0.01463	0.01475	0.01487	0.01498	0.01510	0.01521	0.01533	0.01555	0.01599	0.01642
0.58	0.01076	0.01079	0.01083	0.01089	0.01103	0.01116	0.01129	0.01142	0.01155	0.01168	0.01180	0.01193	0.01205	0.01230	0.01278	0.01325
0.60	0.00855	0.00859	0.00862	0.00869	0.00884	0.00898	0.00912	0.00926	0.00939	0.00953	0.00966	0.00980	0.00993	0.01019	0.01070	0.01120
0.63	0.00529	0.00533	0.00536	0.00544	0.00560	0.00576	0.00591	0.00607	0.00622	0.00637	0.00652	0.00666	0.00681	0.00710	0.00766	0.00821
0.65	0.00312	0.00317	0.00321	0.00330	0.00346	0.00363	0.00380	0.00396	0.00413	0.00428	0.00444	0.00460	0.00476	0.00507	0.00567	0.00625
0.68	−0.00012	−0.00008	−0.00003	0.00007	0.00026	0.00044	0.00063	0.00081	0.00099	0.00117	0.00134	0.00152	0.00169	0.00203	0.00270	0.00334
0.70	−0.00231	−0.00226	−0.00221	−0.00211	−0.00190	−0.00170	−0.00150	−0.00131	−0.00111	−0.00092	−0.00073	−0.00054	−0.00036	0.00001	0.00072	0.00140
0.72	−0.00454	−0.00448	−0.00443	−0.00431	−0.00409	−0.00388	−0.00366	−0.00345	−0.00324	−0.00303	−0.00282	−0.00262	−0.00242	−0.00203	−0.00126	−0.00053
0.74	−0.00681	−0.00675	−0.00669	−0.00657	−0.00633	−0.00609	−0.00586	−0.00563	−0.00540	−0.00518	−0.00495	−0.00474	−0.00452	−0.00409	−0.00327	−0.00248
0.76	−0.00916	−0.00909	−0.00903	−0.00890	−0.00863	−0.00837	−0.00812	−0.00787	−0.00762	−0.00737	−0.00713	−0.00689	−0.00666	−0.00620	−0.00531	−0.00446
0.78	−0.01160	−0.01153	−0.01145	−0.01131	−0.01102	−0.01073	−0.01045	−0.01018	−0.00991	−0.00964	−0.00937	−0.00911	−0.00886	−0.00835	−0.00739	−0.00647
0.80	−0.01416	−0.01408	−0.01400	−0.01384	−0.01352	−0.01320	−0.01289	−0.01259	−0.01229	−0.01199	−0.01170	−0.01142	−0.01114	−0.01058	−0.00953	−0.00853
0.81	−0.01550	−0.01541	−0.01533	−0.01516	−0.01482	−0.01448	−0.01416	−0.01384	−0.01352	−0.01321	−0.01291	−0.01260	−0.01231	−0.01173	−0.01063	−0.00959
0.82	−0.01688	−0.01679	−0.01670	−0.01652	−0.01616	−0.01581	−0.01546	−0.01512	−0.01479	−0.01446	−0.01414	−0.01382	−0.01351	−0.01291	−0.01175	−0.01066
0.83	−0.01832	−0.01822	−0.01812	−0.01793	−0.01755	−0.01718	−0.01681	−0.01645	−0.01610	−0.01575	−0.01541	−0.01508	−0.01475	−0.01411	−0.01290	−0.01175
0.84	−0.01981	−0.01971	−0.01960	−0.01940	−0.01899	−0.01859	−0.01820	−0.01782	−0.01745	−0.01708	−0.01672	−0.01637	−0.01602	−0.01535	−0.01407	−0.01287
0.85	−0.02137	−0.02126	−0.02115	−0.02093	−0.02050	−0.02007	−0.01966	−0.01925	−0.01885	−0.01846	−0.01808	−0.01771	−0.01734	−0.01663	−0.01528	−0.01402
0.86	−0.02301	−0.02289	−0.02277	−0.02254	−0.02208	−0.02162	−0.02117	−0.02074	−0.02031	−0.01990	−0.01949	−0.01909	−0.01870	−0.01795	−0.01652	−0.01519
0.87	−0.02475	−0.02462	−0.02449	−0.02423	−0.02373	−0.02324	−0.02276	−0.02230	−0.02184	−0.02140	−0.02096	−0.02054	−0.02012	−0.01932	−0.01780	−0.01640
0.88	−0.02659	−0.02645	−0.02631	−0.02603	−0.02548	−0.02495	−0.02444	−0.02394	−0.02345	−0.02297	−0.02250	−0.02205	−0.02160	−0.02074	−0.01913	−0.01765
0.89	−0.02856	−0.02841	−0.02826	−0.02795	−0.02736	−0.02678	−0.02622	−0.02567	−0.02514	−0.02463	−0.02412	−0.02364	−0.02316	−0.02224	−0.02052	−0.01894
0.90	−0.03069	−0.03052	−0.03035	−0.03002	−0.02936	−0.02873	−0.02812	−0.02752	−0.02695	−0.02639	−0.02584	−0.02531	−0.02480	−0.02381	−0.02197	−0.02028
0.91	−0.03302	−0.03283	−0.03264	−0.03226	−0.03154	−0.03084	−0.03016	−0.02951	−0.02888	−0.02827	−0.02767	−0.02710	−0.02654	−0.02547	−0.02348	−0.02168
0.92	−0.03558	−0.03536	−0.03515	−0.03473	−0.03392	−0.03314	−0.03238	−0.03166	−0.03096	−0.03029	−0.02964	−0.02901	−0.02840	−0.02723	−0.02509	−0.02315
0.93	−0.03845	−0.03820	−0.03796	−0.03748	−0.03655	−0.03567	−0.03482	−0.03401	−0.03323	−0.03248	−0.03176	−0.03107	−0.03039	−0.02912	−0.02678	−0.02470
0.94	−0.04173	−0.04144	−0.04115	−0.04060	−0.03952	−0.03851	−0.03754	−0.03662	−0.03574	−0.03490	−0.03409	−0.03331	−0.03256	−0.03115	−0.02860	−0.02633
0.95	−0.04556	−0.04522	−0.04487	−0.04421	−0.04294	−0.04174	−0.04062	−0.03955	−0.03854	−0.03758	−0.03666	−0.03579	−0.03495	−0.03337	−0.03054	−0.02808
0.96	−0.05022	−0.04978	−0.04935	−0.04853	−0.04697	−0.04552	−0.04418	−0.04292	−0.04173	−0.04062	−0.03956	−0.03855	−0.03760	−0.03581	−0.03266	−0.02994
0.97	−0.05616	−0.05558	−0.05501	−0.05393	−0.05192	−0.05010	−0.04843	−0.04689	−0.04546	−0.04413	−0.04288	−0.04170	−0.04059	−0.03854	−0.03498	−0.03196
0.98	−0.06448	−0.06361	−0.06277	−0.06120	−0.05840	−0.05593	−0.05374	−0.05176	−0.04996	−0.04832	−0.04679	−0.04538	−0.04405	−0.04165	−0.03756	−0.03416
0.99	−0.07859	−0.07688	−0.07530	−0.07248	−0.06781	−0.06403	−0.06084	−0.05809	−0.05568	−0.05352	−0.05157	−0.04980	−0.04817	−0.04526	−0.04046	−0.03660
1.00	$-\infty$	−0.12752	−0.11357	−0.09961	−0.08566	−0.07750	−0.07170	−0.06721	−0.06354	−0.06044	−0.05775	−0.05538	−0.05326	−0.04958	−0.04379	−0.03930
$\Lambda_1(\Delta E)$		0.01333	0.01339	0.01350	0.01374	0.01396	0.01418	0.01439	0.01459	0.01480	0.01499	0.01519	0.01538	0.01574	0.01645	0.01711
$\Lambda_2(\Delta E)$		−0.02137	−0.02095	−0.02032	−0.01933	−0.01848	−0.01774	−0.01705	−0.01642	−0.01582	−0.01525	−0.01472	−0.01421	−0.01325	−0.01154	−0.01003

TABLE X. Corrections to the Michel ρ_M parameter due to radiative corrections to the one-parameter muon-decay theory.

Momentum range of experiment η_{min}	η_{max}	$(\Delta\rho)$ Berman-BFS	$(\Delta\rho)$ Berman-Michel
0.01	1	0.0086	0.0488
0.11	1	0.0085	0.0449
0.21	1	0.0082	0.0417
0.31	1	0.0076	0.0394
0.41	1	0.0071	0.0382
0.51	1	0.0067	0.0386
0.61	1	0.0066	0.0399
0.71	1	0.0068	0.0412
0.81	1	0.0068	0.0411
0.91	1	0.0063	0.0407

mass of the muon, m_2=rest mass of the electron, $e=2.71828$, and ΔE the energy interval used in the experiment. To pass from one energy interval ΔE_1 to another interval ΔE_2, one can use the relation[3,4]

$$h(\eta,\Delta E_2)=h(\eta,\Delta E_1)+\frac{\alpha}{2\pi}\left\{2\left(2\ln\eta+2w-1-\frac{1}{\eta}\right)\times\ln\left[\frac{(1-\eta)m_1e+2\Delta E_2}{(1-\eta)m_1e+2\Delta E_1}\right]\right\}. \quad (30)$$

Because of a misprint, the factor $\alpha/2\pi$ does not appear in the reference cited as the source of this relation. We have calculated this function $h(\eta,\Delta E)$ for different constant ΔE values. Most of the results of our calculations of this function are presented in Table IX. Also appearing in this table are the evaluated integrals $\Lambda_1(\Delta E)$ and $\Lambda_2(\Delta E)$, where

$$\Lambda_1=4\int_0^1 h(\eta,\Delta E)[3\eta^2(1-\eta)]d\eta,$$
$$\Lambda_2=4\int_0^1 h(\eta,\Delta E)[\eta^3]d\eta. \quad (31)$$

Tables of the function $h(\eta,\Delta E)$ varying by steps of $\Delta\eta=0.01$ were used throughout all our numerical calculations involving this function. A corresponding table based on a definition by Behrends *et al.* of $h(\eta,\Delta E)$ was calculated by us and is given in reference 6.

In Table X we present the necessary increment that must be added to an experimentally measured Michel parameter because of radiative corrections to the theory of muon decay. In the first column we list the range of the experimental momentum interval. Column 2 presents the $\Delta\rho$ increment that should be added to those reported experimental ρ_M values that have already been corrected properly by using the BFS expressions for the radiative correction so as to take into account the Berman modification of these expressions. In Column 3 are the increments $\Delta\rho$ that must be added to a Michel parameter that is determined from experimental data by using the simple one-parameter Michel equation without radiative corrections. These increments are determined by calculations following a minimum-χ^2 procedure whereby the Berman modified Michel curves are compared with a specific one-parameter Michel or Michel-BFS modified curve.

For our calculation of Columns 2 and 3, we define χ^2 as

$$\chi^2=\sum_i \frac{[P(E_i,\rho_M)-M(E_i,\rho_M')]^2}{M(E_i,\rho_M')}, \quad (32)$$

where M represents that particular theoretical curve to which the family of theoretical curves given by $P(E,\rho_M)$ is being compared. All these comparisons are made in the neighborhood of $\rho_M=0.75$. One may now omit the complications introduced into the analysis of the experimental data by the radiative corrections to the one-parameter Michel theory by (a) first determing a value of ρ_{eff} from the experimental data by using the simple theory uncorrected for these radiative corrections, and (b) adding to this ρ_{eff} the $(\Delta\rho)$ Berman-Michel increment from Column 3 of Table X, which corresponds to the momentum range of the experiment to determine the proper Michel ρ_M parameter.

In Table X one notes that for the experimental ranges between $\eta_{min}=0.30$ and $\eta_{max}=1$, the average value of the correction that should be applied to ρ_{eff} determined from the Michel one-parameter equation without radiation correction is lower than the value that one would expect by adding the value 0.007 from Column 2 to the reported value, which is $(0.750-0.706)=0.044$.[30] This difference arises from an overestimate of the original correction in this reported value. The reported difference should have been $(0.750-0.717)=0.033$.[31]

D. Background Determination

In Fig. 7 we have shown the serious effect of background on a magnetic-spectrometer-measured value of ρ_M when pions are created in the target that is also used as the source within the spectrometer of positrons from muon decay. Published values on the variation of pion-production cross section with pion energy[11] illustrate that the desired sources of positrons originate only in a very small pion-energy interval. Pions not in this energy interval leave the production target and embed themselves in the surrounding areas. Those pions that give rise to muons near or at the surface of the spectrometer geometry become an undesirable source of positron background that cannot be distinguished by electronic techniques that measure muon lifetime from positrons that originate in the target. One can screen out some (but not all) of this background. We present the

[30] T. Kinoshita and A. Sirlin, Phys. Rev. **107**, 593 (1957).

[31] This was pointed out also by A. Sirlin in a letter to S. Bludman (May 18, 1958). Sirlin's new calculations give an 0.040 increment that should be added to ρ_{eff}. This is in good agreement with values appearing in Table X. [See T. Kinoshita and A. Sirlin, Phys. Rev. (to be published)].

procedures that were used to estimate this background in our experiment, along with other corrections that must be considered in our reduction of the raw data. We present these in the order of increasing influence on the reported data.

1. *Correction For Electron Scattering in the Detector*

Figure 20 illustrates the experimental procedure that was used to measure the correction for electron scattering in the detector. This information was obtained by use of a scattered beam of electrons created by photons from a 330-Mev synchrotron. As shown in this figure, an additional thickness t' of scintillator material was introduced directly in front of the first counter, and quadruple coincidences were measured. The ratio (with its standard deviation) of the number of these coincidences when thickness t' was present to the number when it was absent was determined, and is plotted for various thicknesses t' in Fig. 20. These measurements were made at two E_0' energy settings, which define the positron-energy interval in which this correction would most seriously affect the measured ρ_M value. We draw the conclusion that within the statistics of these measurements no correction is necessary for positron scattering in our detector.

2. *Effect of Muon-Density Distribution*

An effect that could seriously change the resolution of the spectrometer and therefore the determined value of ρ_M is the distribution of muons within the target. We tested for this effect in our experiment by changing the size of the incident collimated proton beam (from $\frac{1}{2}$ in. in diameter to $\frac{3}{4}$ in. in diameter). This was done first for a lithium target $2\frac{3}{8}$ in. in diameter and then for a target 1 in. in diameter. In both cases we found no significant changes in our intensity measurements that would arise from a possible variation of muon density. Table XI illustrates this with the raw data obtained by use of the $2\frac{3}{8}$-inch target.

We conclude that within the statistics of these measurements and the accuracy of the assumed variations in our calculations leading to the conclusion shown in Table VI, the assumption of a uniform muon-density distribution within the target introduces no serious systematic error in the calculation of our spectrometer resolution functions (Appendix A).

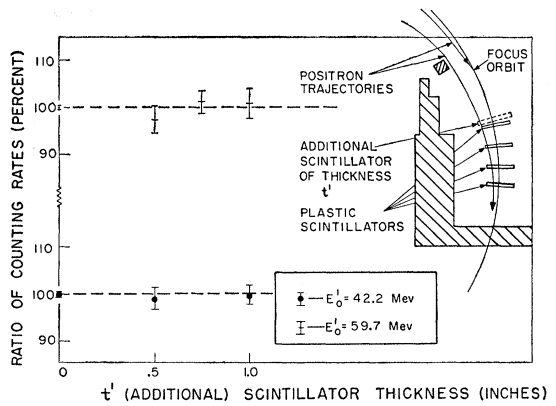

FIG. 20. Results from the experimental study of the correction to the measured intensity for positron scattering in the detector.

TABLE XI. Intensity measurements for beams of different sizes (counts minus accidental background divided by magnetic field).

	Diameter of collimated proton beam			
	$\frac{1}{2}$ inch		$\frac{3}{4}$ inch	
E_0'	$X(E_0')$	σX	$X(E_0')$	σX
32.9	9.19	0.16	9.17	0.30
46.9	9.85	0.08	9.63	0.26
50.5	6.10	0.11	6.15	0.21

3. *Pion "Flyback-Effect" Background*

In our experiment there are pions that leave the target and remain trapped by the magnetic field in the region between the target and the detector (Fig. 2), or are returned to the target before the positron is born. The number of these pions varies with the magnetic field strength. We give the name "flyback effect" to the influence of the positrons that originate from these pions on the measured intensities at the various E_0' values. We have calculated the effect of this source of positrons on the resolution of the spectrometer. We find that it becomes significant only when the proton-beam diameter is larger than the target diameter and at the same time the target diameter is very small. The target and proton-beam conditions that were chosen for the measurement of the ρ_M parameter were such as to render negligible the effect of this variable positron source (Table VI).

In addition to our calculations of the influence of the flyback effect on the resolution, we have conducted an experiment that could measure its presence. By reversing the polarity of the magnetic field one brings electrons into focus at the detector position. The sources of these delayed electrons are the negative muons that arise from the decay of negative pions experiencing the same trajectories in this magnetic region. From measurements of negative and positive pion-production cross sections at low pion energies (as shown in reference 11), a ratio of positive to negative pions is determined for the small range of energy for pions that give rise to the muons that decay into positrons and electrons. With this ratio and the electron measurements one can estimate the contribution to the measured positron intensities of the flyback effect at each E_0' value. These measurements were made at three E_0' values. Our estimate of the contribution was approximately 0.2%. Calculations yielded values less than 0.1% for the targets that were used.

4. *Background Due to Pions Stopping in the Detector*

There are, within a very small low-energy interval, pions that satisfy the same focusing conditions as do

the desired positrons. The energy of these pions is not sufficient to penetrate through the first scintillator until the energy setting of the spectrometer exceeds the maximum energy of positrons originating in the target. From these pions, positrons eventually arise that have a large probability of triggering the electronic system. If one neglected the effect of this positron source and if it were significant, it would result in an overestimate of the ρ_M parameter.

We have measured the magnitude of this positron source, at three E_0' values, by the following procedure. First the spectrometer resolution was determined for pions that would reach the detector at the chosen E_0' positron-energy setting. This resolution function was used to decide on the thickness of a CH_2 pion-energy degrader that should be used at this E_0' setting to degrade the energy of these pions sufficiently that they would be deflected by the magnetic field and miss the first counter. As shown in Fig. 2, intensity measurements were made with absorber in and absorber out. Our measurements showed that the positron intensity with absorber in was 1% less than the intensity with absorber out at positron energy settings of $E_0'=33$ and 48 Mev. No change in the intensities was observed at $E_0'=58$ Mev, at which positron setting the pions have sufficient energy to pass through the first counter. These measurements were accurate to 2%. We give significance to these measurements because at the two positron-energy settings ($E_0'=33$ and 48 Mev) both positron-intensity measurements with CH_2 absorber in were low. In the reduction of our raw data a constant 1% background was attributed to this effect over the measured range of positron energies below $E_0'=58$ Mev. Because this effect was small in our experiment, we ignored the slow increase of this background with increasing E_0' settings. The increase of this background results from the increase in the pion-production cross section in this pion energy region.

5. *Background from Pions Stopping in Pole Tips*

The largest contribution to the background arises from pions stopping in the pole tips of the spectrometer. Equations expressing the focusing properties of the spectrometer show that the probability of particle detection increases with a decrease of the radius r_0 of the particle source, which is measured from the axis of magnetic symmetry. The contribution of this background to the measured positron intensities can be determined experimentally. Our procedure for measuring this contribution is illustrated in Fig. 21. In addition to this illustration Figs. 1 and 2 are an aid to an understanding of the experimental procedure.

Shown in Fig. 21 is the configuration of the source that is used in these measurements. The original lithium target is positioned inside a thick-walled hollow cylindrical shield made of lead. This assembly is mounted on one side of the median plane of the spectrometer. The wall of the lead cylinder is 2.5 in. thick. This thickness is sufficient to stop (a) all positrons originating in the target that would be focused into the detector, (b) all pions that are created in the target and are emitted into space on the source side of the median plane (except those passing out from the magnet), and (c) all positrons eventually arising from pions that stop in the lead shield. Pions emitted by the target into space opposite to the source side of the median plane embed themselves in the pole of the spectrometer. Some of the positrons that eventually arise because of the presence of these pions at the pole are focused into the detector.

We were able to make significant measurements of the contribution of this background to the measured intensity because of the large-solid-angle focusing property of a spiral-orbit spectrometer. Measurements of this contribution as obtained by this method for one spectrometer geometry[32] ($\Theta'=35°$; $2\frac{3}{8}$-inch-diameter lithium target) are shown in Fig. 20. The best polynomial that represents this set of data was obtained by least-squares fitting and minimum-χ^2 methods. We treated the result that arose from this polynomial expression as one-half the contribution of this background to the measured intensity at the desired E_0' value. As seen, the effect of this background on the raw data is very significant in our experiment. Were this background contribution ignored, the reported ρ_M value (as shown in Fig. 7) would have been between 0.68 and 0.70.

6. *Background from Pions Stopping in the Counter Shield*

The most uncertain background in our experiment results from pions stopping in the lead shield that screens the counters from the secondary particles that are produced during target bombardment by a proton pulse (Figs. 2 and 22). In one of our unreported

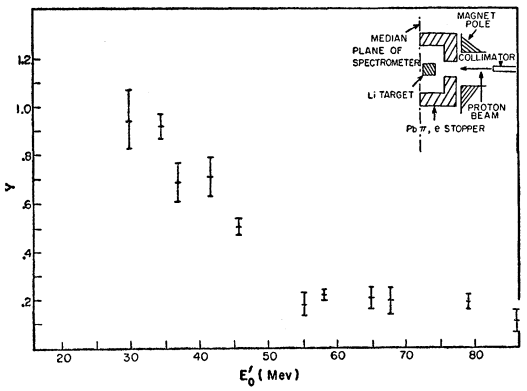

FIG. 21. Measured background from pions stopping in spectrometer pole faces as a function of positron energy at the focus orbit. $\Theta=35°$, $2\frac{3}{8}$-in. target.

[32] Data used for reduction of results in another spectrometer geometry ($\Theta'=35°$; 1-inch-diameter lithium target) are given in reference 6.

experiments we tried to eliminate this lead shield. Our true counting rates were thereupon seriously impaired by the necessary increase in the delay time between the proton pulse and the first gate during which counts were collected. In addition, the background contribution to the measured intensities from pions stopping in the magnetic poles also increased. Because of these serious disadvantages we chose to use this lead shield in our experiments.

It is not practical to directly measure the contribution of this background to the raw data. Therefore we resort to the following computed calculations to determine its magnitude. First the resolution for the system is determined as shown in Fig. 22. For this study a uniform positron-source distribution is assumed over the face of the lead shield exposed to positive pions and over all trajectories studied. More complex trajectories, which are not shown in Fig. 22, were also considered. These contribute very little to the resolution function. Then, this resolution is folded into a modified Michel ($\rho_M=70$) distribution [Eq. (4)], and a curve representing the behavior of the intensity of this background with positron-energy setting E_0' is obtained. We refer to this as unnormalized computed background $Q(E_0')$. It is very flat over the positron-energy intervals that are considered, with a peak occurring at approximately 50 Mev. For the geometry $\Theta'=35°$, $2\frac{3}{8}$-inch target diameter (see Fig. 7), it contributes roughly 45% to the total background at electron energies $\geqslant 55$ Mev. At electron energies of about 30 Mev its contribution is approximately 14%. We determine the magnitude of this background at energies $E_0'<50$ Mev by establishing the normalization factor for $Q(E_0')$ from measurements made, during the regular experiment, of total background beyond the E_0' energy cutoff of the desired spectrum, as shown in Fig. 7. Background measured above $E_0'=56.5$ Mev originates from two sources, (a) from pions stopping in the pole faces of the magnet (which is separately measured) and (b) from pions stopping in the lead shield protecting the counters.

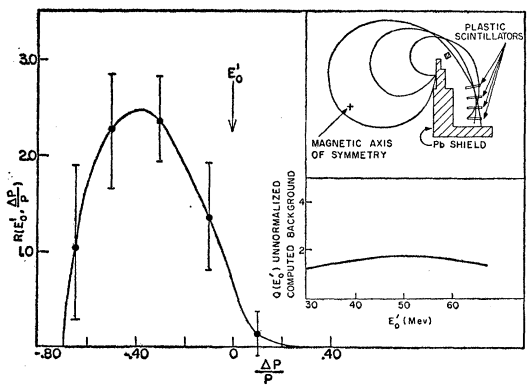

FIG. 22. Magnetic resoultion for a broad positron source resulting from pions stopping in the lead detector shield.

In establishing the normalization factor the computer executed the following series of instructions.

1. By a series of repeated calculations, a polynomial

$$\sum_{k=0}^{m} a_k x^k$$

was fitted to the data representing the pole-face background (Fig. 21). In this least-squares fitting the data were weighted by the square of the reciprocal of the plotted standard deviations. For each value of m, a χ^2 value was determined. The value of m could range between zero and 14. The polynomial (where m was not equal to the number of points) that yielded the minimum χ^2 value was chosen to represent these data. Let us call this polynomial $y_1(E_0')$.

2. In a similar way a polynomial $y_2(E_0'\geqslant 56.5)$ was determined to represent the total experimental background shown in Fig. 7 above $E_0'\geqslant 56.5$ Mev.

3. Then the polynomial y_3, which best represents the difference y_2-2y_1, was determined in the region $E_0'\geqslant 56.5$ Mev. We multiply y_1 by 2 in obtaining this difference because the data shown in Fig. 21 are for one magnet pole face. The polynomial y_3 represents the background contribution to the measured intensities above $E_0'=56.5$ Mev from the lead shield protecting the counters.

4. The area under the computed background $Q(E_0')$ was calculated above $E_0'=56.5$ Mev and normalized to the area under the function y_3, and a χ^2 value was determined. Because no positron ionization or radiation loss was introduced into the determination of the resolution given in Fig. 22, we accounted roughly for them by shifting the energy scale of the distribution $Q(E_0')$ and, as before, normalizing and determining the χ^2 value. That normalization factor and energy scale which yielded the minimum χ^2 in this comparison of the distribution $Q(E_0')$ and y_3 was taken as the desired one. The final computer calculation was the subtraction of these backgrounds from the raw data, yielding the reduced data after a multiplication by a normalization constant (Figs. 8, 9, and 10).

It is of interest to point out the effect on the Michel parameter of a systematic error in the normalization factor for this computed background. Consider a large change that is not justified by the background measurements that have been made. As an example, a 50% increase or decrease of the computed background would require approximately a 40% change in the measured background in the energy region in which the normalization factor for the computed background is determined ($E_0'>56.5$ Mev).

We summarize the results from the study of this effect in Table XII, where we present in Column 1 the amount of calculated background as related to that actually used (i.e., 100% corresponds to the optimized condition as selected by the computer) in our reduction of the data; in Column 2, the value of ρ_M that arises from the

TABLE XII. Effect of computed background on the ρ_M parameter.

Amount of computed background present (%)	ρ_M	$\Delta\rho$	Comment
50	0.764	+0.019	Assumption
100	0.746±0.035		Optimized background selected by computer
150	0.723	−0.023	Assumption
200	0.711	−0.034	Assumption

minimum-χ^2 determination for the chosen background; and in Column 3, the amount of $\Delta\rho$ that would have been added to the ρ_M value (as shown in Fig. 8) if the chosen assumption were true.

E. Time-Scale Calibration for Determination of Muon Mean Lifetime

The determination of the muon mean lifetime depends on knowing the time widths of the gates and the dead times between them; these times establish that particular moment—which we call the instant of the mean counting rate—at which we could represent by an instantaneous counting rate all the counts occurring within the duration of any one gate. (Because of the finite lifetime of the particles, this time of the mean counting rate occurs before the midpoint of the gate duration). We define the time from "zero" up to this moment as the sum of (a) the delay, after the proton pulse, of the start of the first gate, (b) the total of the time widths and dead times between the gates of all the foregoing gates, and (c) the time from the start of the gate in question until the instant of the mean counting rate.

The absolute measure of Time (a) is not important for a lifetime measurement. Its setting is governed by the magnitude of the accident counting rate. We have measured Interval (b) by photographing the active time of each gate and the dead time between gates on a calibrated time scale. For a measure of the gate width the sine wave of a 10-megacycle Tektronix time-mark generator (accuracy 50 cycles per megacycle) was fed into the amplifier section of a Tektronix 517 oscilloscope. The amplified signals were then used as input into the tandem gate unit. A Berkeley Instruments double-pulse generator triggered the tandem gate and also the sweep circuit of another 517 Tektronix oscilloscope on which the output from each gate was displayed. The display of each individual gate width was photographed together with the superimposed sine wave. Approximately twenty such oscilloscope displays were photographed for each gate. Under magnification we could see that the error of measuring the number of sine waves displayed during the active time of the gate was less than one-half cycle. For each gate the active time was defined as the time between the half height of the voltage ordinate during the start of the gate and that at the cutoff. In our reduction of the data we used the time width of each gate and its error as obtained from the arithmetic mean of these measurements. Each gate width was approximately 2 microseconds. The gate widths of the four gates were the same within 5%.

The dead time between adjacent gates was measured in the same manner except for small modifications. In this measurement the sine wave of a 50-Mc Tektronix time-mark generator was used. The signal from this source was fed directly to the oscilloscope. Superimposed on the same photograph were the rise and cutoff portions of the two adjacent gates. The number of sine waves displayed during the nonactive time between gates was measured under magnification. The arithmetic mean of such measurements was used as the dead time between gates.

Interval (c) is obtained by a calculation relating the counting rate for the measured gate width to the instantaneous counting rate corresponding to the decay rate for particles having the mean life in question. For exactly equal gate time widths no error is introduced in calculating the time of Interval (c) by the assumed value of the mean life, because a measurement of the lifetime is independent of the origin of the time scale. An error of 10% in the assumed mean life introduces a shift of approximately 1% in the time given by Interval (c) for our system. Because the gate time widths in our system are approximately equal, a 10% variation of the assumed mean life introduces a maximum error of 0.001 μsec in the time used for a particular gate. These errors, corresponding to errors in the time of the mean counting rate of a gate, do not influence the data appearing in Table III.

In the treatment of our data we simplified our calculations of the mean life by considering that there was no error in the timer of the mean counting rate. This simplification introduces a maximum additional error of 0.005 μsec in the mean life. This error is in addition to that obtained from a statistical treatment of the data in which errors from the time widths of gates and the number of counts are taken into account. We have allowed for this additional error in reporting the accuracy of the weighted mean value of the mean life as given in Table III.